Experimental Determination of Vibrational Potential Energy Surfaces and Molecular Structures in Electronic Excited States

1 AUTHOR:

Jaan Laane
Texas A&M University

265 PUBLICATIONS **4,232** CITATIONS

SEE PROFILE

FEATURE ARTICLE

Experimental Determination of Vibrational Potential Energy Surfaces and Molecular Structures in Electronic Excited States

Jaan Laane

Department of Chemistry, Texas A&M University, College Station, Texas 77843

For more than three decades far-infrared and Raman spectroscopies, along with appropriate quantum mechanical computations, have been effectively used to determine the potential energy functions which govern the conformationally important large-amplitude vibrations of nonrigid molecules. More recently, we have utilized laser-induced fluorescence (LIF) excitation spectroscopy and ultraviolet absorption spectroscopy to analyze the vibronic energy levels of electronic excited states in order to determine the potential energy surfaces and molecular conformations in these states. Transitions from the ground vibrational state in an S_0 electronic state can typically be observed only to several excited vibronic levels. Hence, the LIF of the jet-cooled molecules generally provides data on only a few excited state levels. Ultraviolet absorption spectra recorded at ambient temperatures, however, often provide data on many additional excited vibronic levels. However, these can only be correctly interpreted if the electronic ground state levels have been accurately determined from the far-infrared, Raman, and dispersed fluorescence studies. In this article, we will first present our results for bicyclic molecules in the indan family in their S_0 and $S_1(\pi,\pi^*)$ electronic states. Two-dimensional potential energy surfaces in terms of the ring-puckering and ring-flapping vibrations were utilized for the analyses. Next, we review our work on *trans*-stilbene in its S_0 and $S_1(\pi,\pi^*)$ states and examine the data from which two-dimensional potential energy surfaces were determined for the phenyl torsions and one-dimensional functions were calculated for the torsion about the C=C bond, which governs the photoisomerization. Finally, we consider seven cyclic ketones in their S_0 and $S_1(n,\pi^*)$ states. The carbonyl wagging vibration of each was studied in its electronic excited state in order to determine the barrier to inversion and the wagging angle. The barrier to inversion was found to increase with angle strain. Conformational changes between the ground and excited electronic states were also examined in terms of the out-of-plane ring motions.

1. Introduction

Numerous molecular processes such as isomerization or inversion proceed along vibrational pathways that are governed by vibrational potential energy surfaces. In selected cases, these surfaces can be described very well by just one or two vibrational coordinates. This is generally based on the high−low frequency separation: conformational changes typically are associated with low-frequency anharmonic, large-amplitude vibrations which interact little with higher frequency modes. Over the past three decades we have studied numerous four-, five-, and six-membered ring molecules as well as bicyclic systems using far-infrared and Raman spectroscopy.[1−4] The ring-puckering vibrations (Figure 1) for molecules such a cyclobutane, cyclopentene, and 1,4-cyclohexadiene can be represented very well by a single vibrational coordinate (*x*) in each case, and potential energy functions of the form

$$V = ax^4 + bx^2 \qquad (1)$$

when used in the Schrödinger equation, do an excellent job of fitting the experimental spectroscopic data. The potential energy parameters *a* and *b* can be related to the intramolecular forces

and geometry of the molecule. The molecules shown in Figure 1 are a four-membered ring and two "pseudo-four-membered rings" where the atoms connected by double bonds behave as single units during the puckering vibrations. For molecules such as cyclopentane and cyclohexene, which are not pseudo-four-membered rings, two-dimensional potential energy surfaces have been used to represent the conformational energetics. These generally have the form

$$V(x_1,x_2) = a_1 x_1^4 + b_1 x_1^2 + a_2 x_2^4 + b_2 x_2^2 + c x_1^2 x_2^2 \quad (2)$$

where x_1 and x_2 are the vibrational coordinates (such as ring-bending and ring-twisting) and a_1, b_1, a_2, b_2, and c are the potential energy parameters. This potential energy function is also applicable for several types of bicyclic molecules and can also be used to refine the calculations for the pseudo-four-membered rings when small interactions with other vibrations are to be accounted for.

During the past decade we have been concentrating our efforts on determining the potential energy surfaces of electronic excited states using laser-induced fluorescence (LIF) spectroscopy of supersonic jet-cooled molecules and ultraviolet absorption
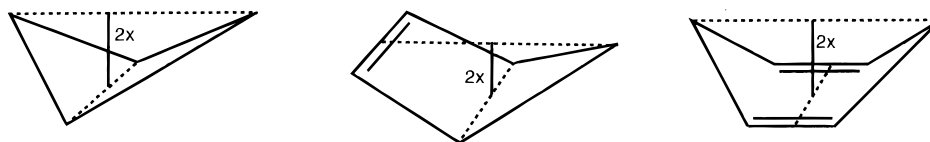
Figure 1. Ring-puckering coordinate for cyclobutane, cyclopentene, and 1,4-cyclohexadiene.

spectroscopy. Despite the added complications expected for the excited states, the same process of mapping the vibrational quantum states and using these to determine the potential energy surfaces has worked remarkably well.

In this review, we will examine the potential energy surfaces and structures of the bicyclic molecules in the indan family, of stilbenes, and of various cyclic ketones. In each case, data for both the ground and excited electronc states will be examined since the former are required for the proper analysis of the excited states.

2. Theory

In 1945 Bell[5] predicted that the ring-puckering vibration of a four-membered ring should be governed by a quartic oscillator function ($b = 0$ in eq 1). Laane[6] has shown that the parameters in eq 1 for cyclobutane can be related to the ring-angle-bending force constant k_ϕ, the initial angle strain S_0, and the C—C bond distance R, by

$$a = 128 k_\phi/R^4 \tag{3}$$

$$b = 32 k_\phi S_0/R^2 \tag{4}$$

These contributions are both positive and hence would result in a planar ring with the energy minimum at $x = 0$. However, for cyclobutane and other molecules, the torsional forces, which result from $-CH_2-CH_2-$ interactions and other effects, often produce a substantial negative contribution to the parameter b, and this can result in a double-minimum potential energy function and a nonplanar ring molecule.

The one-dimensional Schrödinger equation for a vibration with a fixed reduced mass μ is

$$(-\hbar^2/2\mu)\, d^2\psi/dx^2 + V\psi = E\psi \tag{5}$$

This can be transformed to the reduced form[7] using

$$Z = (2\mu/\hbar^2)^{1/6} a^{1/6} x \tag{6}$$

$$E = A\lambda \tag{7}$$

$$A = (\hbar^2/2\mu)^{2/3} a^{1/3} \tag{8}$$

$$B = (2\mu/\hbar^2)^{1/3} a^{-2/3} b \tag{9}$$

This results in

$$-d^2\psi/dZ^2 + (Z^4 + BZ^2)\psi = \lambda\psi \tag{10}$$

where Z is the dimensionless coordinate. B defines the quadratic contribution which may be positive or negative, and the λ are the eigenvalues which are proportional to the vibrational quantum states E. Each value of B defines a set of eigenvalues which may be computed and then scaled by the parameter A to best fit the experimental data. Hence, the effective potential energy function is

$$V = A(Z^4 + BZ^2) \tag{11}$$

Figure 2 shows the first 17 eigenvalues calculated for this function for different values of B (with $A = 1$). For $B = 0$ the function is that of a pure quartic oscillator. For positive B a mixed quartic/quadratic function exists with a pure harmonic oscillator approached as $B \rightarrow \infty$. When B is negative, the function represents a double minimum potential with a barrier of $B^2/4$, and pairs of energy levels begin to merge below the barrier. When $B \rightarrow -\infty$, the pairs of energy levels become equally spaced and also approach those of a harmonic oscillator. Figure 3 shows the experimentally determined potential energy function for the ring-puckering vibration of several different molecules with values of B ranging from $B = +4.68$ to -9.33. 2,5-Dihydrothiophene[8] (DHT) has a mixed quartic/quadratic potential ($B = 4.68$) while 3-silacyclpent-1-ene[9] (SCP) is a nearly perfect quartic oscillator with $B = -0.17$. Both molecules are planar. Trimethylene oxide[10] (TMO), 1,3-disilacyclobutane[11] (DSCB), cyclopentene[12] (CP), and silacyclobutane[13] (SCB) have increasingly negative B values (-1.47, -4.65, -6.17, and -9.33, respectively) and increasing barriers to planarity. Their potential energy functions show how energy levels merge to produce "inversion doubling." As the barrier increases, more and more levels can be seen to begin merging. Figure 2 indicates the B value corresponding to the molecules whose functions are shown in Figure 3. The eigenvalues at those specific B values correlate to the energy levels on the potential energy curves when the appropriate scaling factor A is used.

Many of the original ring-puckering studies utilized the wave equation (eq 5) to fit the experimental data. However, since this vibration has a large amplitude and the reduced mass changes with the vibrational coordinate, the calculations can be improved by utilizing a computed reduced mass function which depends on the coordinate. In one-dimension the Hamiltonian becomes

$$\mathcal{H}(x) = (-\hbar^2/2)\partial/\partial x(g_{44}(x))\partial/\partial x + V(x) \tag{12}$$

where g_{44} is the coordinate-dependent reciprocal reduced mass function that can be represented by a polynomial

$$g_{44} = g_{44}^{(0)} + g_{44}^{(2)}x^2 + g_{44}^{(4)}x^4 + g_{44}^{(6)}x^6 \tag{13}$$

The odd-powered terms in this polynomial representation are usually zero (if puckering up and down are equivalent). Only terms up through the sixth-power term are included. The subscripts on g_{44} reflect the fact the values $1-3$ are reserved for the molecular rotations. As shown by Malloy,[14] the reduced mass for the puckering motion can be readily calculated at different coordinate values using vector methods. The difficult part is to correctly model the vibrational motions. Laane and co-workers[15−19] have described the computation of the kinetic energy expressions for several different types of vibrations using vector methods for both one- and two-dimensional cases. In two dimensions, the Hamiltonian becomes

$$\mathcal{H}(x_1,x_2) = -(\hbar^2/2)[\partial/\partial x_1(g_{44}(x_1,x_2))\partial/\partial x_1 + \\ \partial/\partial x_2(g_{55}(x_1,x_2))\partial/\partial x_2 + \partial/\partial x_1(g_{45}(x_1,x_2))\partial/\partial x_2 + \\ \partial/\partial x_2(g_{45}(x_1,x_2))\partial/\partial x_1] + V(x_1,x_2) \tag{14}$$

Feature Article

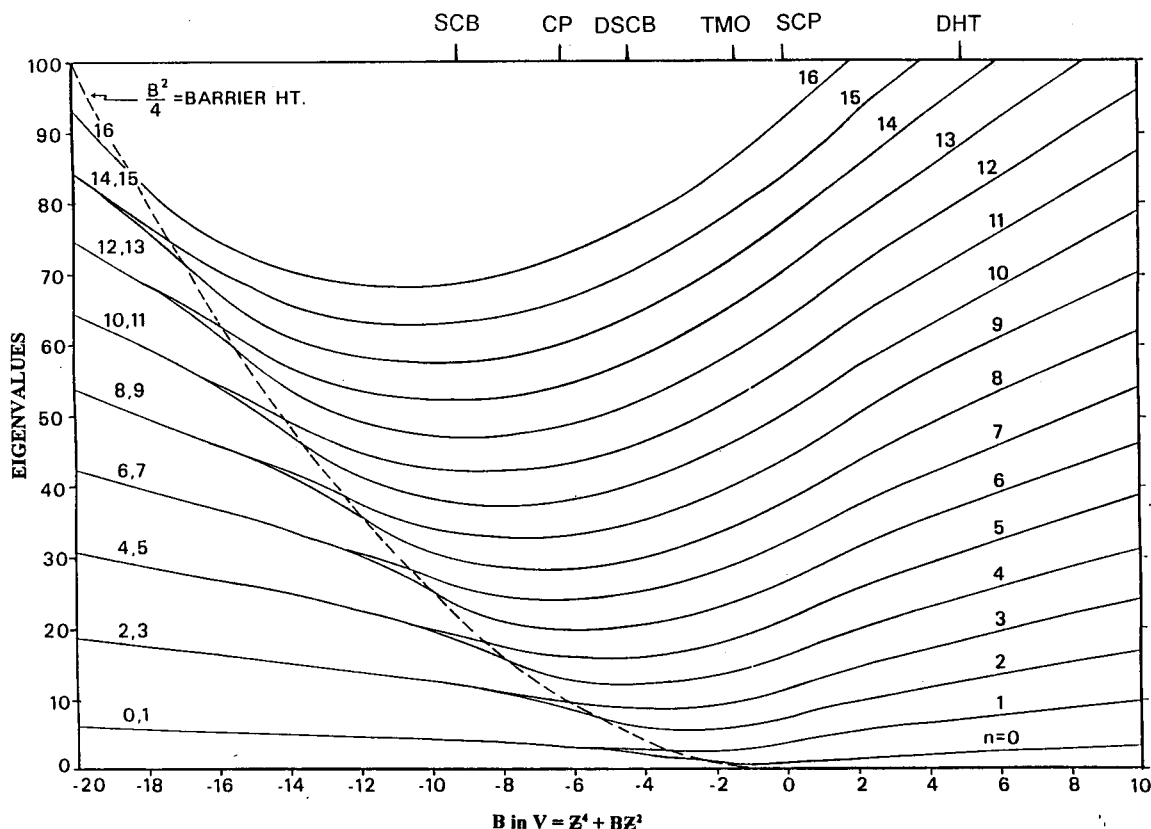*J. Phys. Chem. A, Vol. 104, No. 33, 2000* **7717**

Figure 2. Eigenvalues for the reduced potential energy function $V = Z^4 + BZ^2$ as a function of B. The B values of the molecules shown in Figure 3 are indicated.

where $V(x_1,x_2)$ typically has the form of eq 2. The $g_{ij}(x_1,x_2)$ are calculated as a function of both coordinates, again using vector methods. Utilization of these kinetic energy functions rather than a fixed reduced mass tends to affect the potential energy parameters by less than 5% but does reduce the deviation between observed and calculated frequencies by about a factor of 2 (typically from an average 1 to 2 cm^{-1} deviation for the fixed reduced mass model to half of that).

3. Experimental Methods

Figure 4 shows some of the spectroscopic transitions and experimentally determined energy levels for both the ground (S_0) and first excited $S_1(\pi,\pi^*)$ electronic states of phthalan, a molecule to be discussed later. The diagram shows far-infrared absorption and Raman transitions which are used to determine the vibrational quantum states for the electronic ground state. These generally have changes of $\Delta v_P = 1$ and 2, respectively, for the major transitions of the ring-puckering vibration. Laser-induced fluorescence (LIF) of the jet-cooled molecules results from transitions which for the most part originate from the vibrational ground state in S_0. However, if the molecular jet is warmed somehat, weak transitions from the $v_P = 1$ state (30.9 cm^{-1} above the ground state) can also be seen. With LIF the laser system is tuned and when the energy of the vibronic level is reached, the fluorescence signal is detected (fluorescence excitation spectra). For molecules excited from the $v_P = 1$ level fluorescence results when the frequency matches the separation between $v_P = 1$ and the vibronic level. The ultraviolet absorption spectra are recorded at room temperature and hence transitions can originate from up to a dozen of the S_0 vibrational levels. The C_{2v} symmetry of phthalan restricts which transitions are allowed and this explains why only $v_P =$ even to even or odd to odd transitions are observed. The LIF spectra are most

valuable in that they clearly show which transitions originate from the vibrational ground state. However, the Franck−Condon factor limits the number of S_1 vibronic states that can be accessed. In these cases the ultraviolet absorption spectra are most helpful in that many of the higher vibronic states can be reached only when the transitions originate from upper vibrational levels in S_0. The ultraviolet absorption spectra in our laboratory are recorded on a Bomem 8.02 Fourier transform spectrometer. The laser-induced fluorescence system utilizes a Nd:YAG laser to drive either a dye laser or an optical paramagnetic oscillator. The molecules are cooled through a supersonic jet expansion using a pulsed valve. Detection is with a photomultiplier tube (PMT) or by a time-of-flight mass spectrometer. Dispersed fluorescence spectra can also be recorded using PMT or CCD detection. More detail can be found elsewhere.[20−22]

4. Results and Discussion

A. Bicyclic Molecules in the Indan Family. The molecules indan, phthalan, coumaran, and 1,3-benzodioxole shown below are "pseudo-four-membered-ring" molecules since the ring-puckering vibration resembles that of a four-membered ring (or cyclopentene) in that the two atoms of the five-membered ring that are also part of the benzene ring tend to move together.
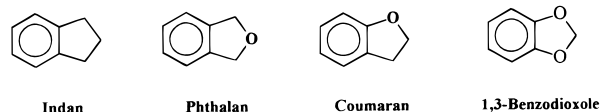
However, because each molecule is bicyclic, there is a low-frequency ring-flapping vibration (also called the butterfly motion) of the same symmetry species as the ring puckering
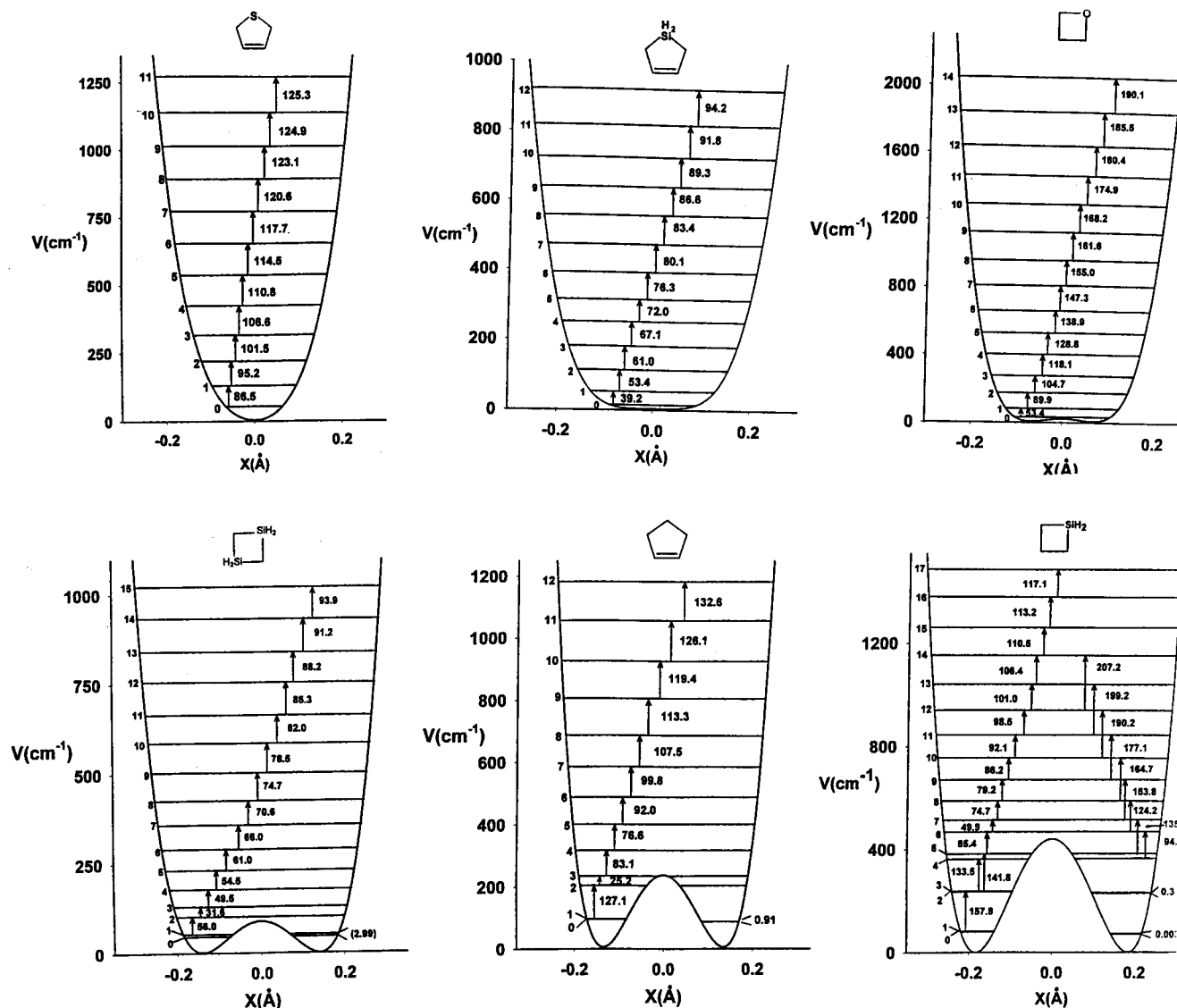
Figure 3. Potential energy functions for the ring-puckering vibration of several different molecules. The values of B in eq 11 are as follows for the indicated molecules: DHT (4.68), SCP (−0.17), TMO (−1.47), DSCB (−4.65), CP (−6.17), SCB (−9.33).
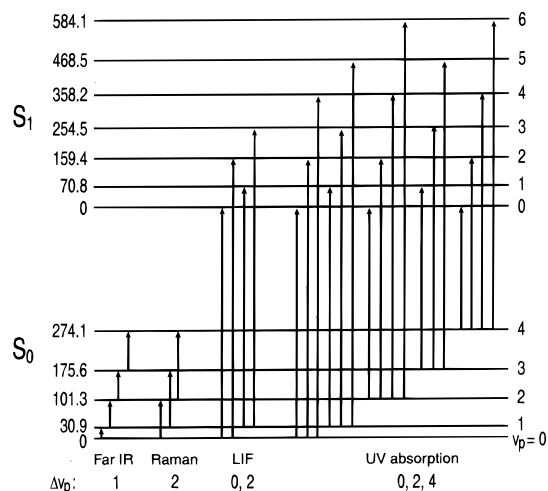

Figure 4. Spectroscopic transitions involving the ground and excited electronic states of phthalan.

Figure 5. Definition of the ring-puckering (x_1) and ring-flapping (x_2) coordinates for indan and related molecules.

rings. The flapping (x_2) is the motion of the entire five-membered ring relative to the benzene ring. The figure shows the motions from a side perspective relative to the plane of the benzene ring. Atoms 4 and 5 are the carbon atoms common to both rings. Atoms 1, 2, and 3 are in the five-membered ring.

Vector methods have been developed to represent the motion of all the atoms relative to x_1 and x_2 so that the kinetic energy (reciprocal reduced mass) expressions for the molecules can be calculated as a function of the coordinates.[23,24] Figure 6 shows how g_{44}, the reciprocal reduced mass function for phthalan, varies as a function of coordinates, and the coordinate dependence can be seen to be substantial.[24]

Our results for both the electronic ground and excited states of phthalan[24,25] and 1,3-benzodioxole[26,27] are presented below. The ground state investigation of coumaran[28] is also discussed. The preliminary FES and UV absorption spectra of coumaran have also been recorded in our laboratory but will not be

that can interact strongly with the puckering. Figure 5 shows the definition of these two low-frequency motions. The puckering (x_1) is basically the out-of-plane motion of the apex CH_2 group or oxygen atom relative to all the other atoms in the two
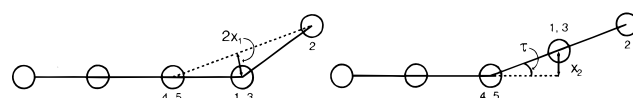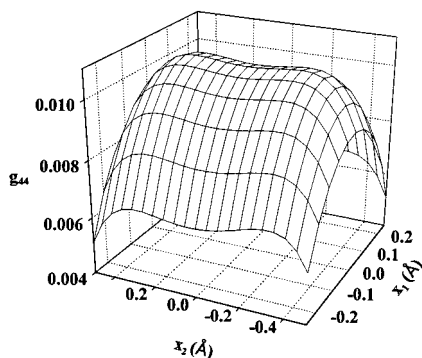
Feature Article

J. Phys. Chem. A, Vol. 104, No. 33, 2000 **7719**

Figure 6. Dependence of reciprocal reduced mass g_{44} for the ring-puckering of phthalan on the x_1 and x_2 coordinates.
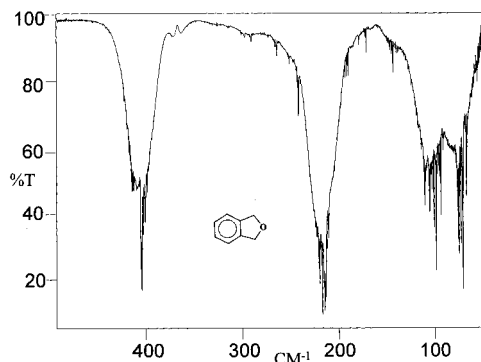

Figure 7. Far-infrared spectrum of phthalan vapor.

Figure 8. Energy level diagram for the ring-puckering vibration (v_P) in different ring-flapping (v_F) states of phthalan.

Figure 9. One-dimensional ring-puckering potential energy function calculated for phthalan.

reported here. As has been noted previously,[29] the coumaran spectra for the excited state are complicated by dimerization. Spectroscopic work on both the ground and excited states of indan is also in progress in our laboratory. Previous ground[30] and excited[31] state assignments clearly need revision. A recent microwave study proposes a barrier of 444 cm^{-1} based on the ground state splitting,[32] much lower than the originally reported value[30] of 1979 cm^{-1}. A high-level ab initio calculation predicts a barrier of 662 cm^{-1}. In the $S_1(\pi,\pi^*)$ state the barrier is clearly lower as the $0 \rightarrow 3$ transition drops from 143.2 to 112 cm^{-1}.

Phthalan S_0 Ground State. Figure 7 shows the far-infrared spectrum of phthalan vapor in the 60−440 cm^{-1} region (20.25 m path, 0.55 Torr pressure).[23] A group of weak bands in the 30−35 cm^{-1} region are also present. The absorption bands originate from transitions between the ring-puckering (v_P) or ring-flapping (v_F) quantum states or both. The $\Delta v_P = 1$ bands were observed in the 30−110 cm^{-1} region for $v_F = 0$, 1, and 2. The double ($\Delta v_P = 2$) and triple ($\Delta v_P = 3$) quantum transitions are weak but were detected in the 100−210 and 175−320 cm^{-1} regions, respectively. Most of the intensity near 220 cm^{-1} is the result from various $\Delta v_F = 1$ transitions with $\Delta v_P = 0$ but arising from different puckering levels. Figure 8 shows the energy level diagram for phthalan for these two vibrations in the S_0 state. The energy level separations for the puckering can be seen to change by moderate amounts in the different flapping states. An attempt was made to fit the observed puckering data using a one-dimensional function of the type in eq 1, but the frequency agreement was not very good, clearly reflecting the fact that the puckering cannot be considered as a motion independent of the flapping. Figure 9 shows the one-dimensional function which gave the best frequency fit along with the observed and calculated transition frequencies.[23] The reason for showing this is to show how poorly the function reproduces the frequency increase from 74.3 to 98.5 cm^{-1} and then back to 93.2 cm^{-1}. A one-dimensional function can only produce
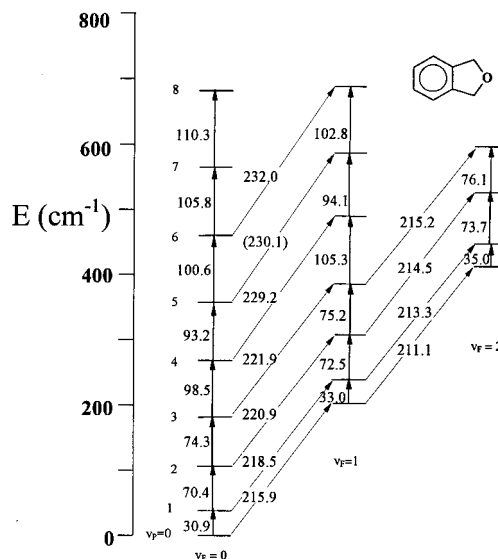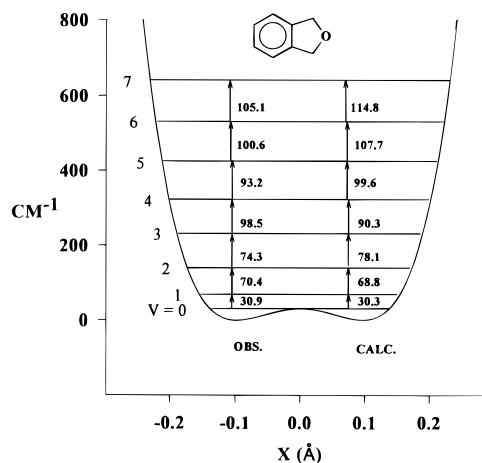
the regularly increasing sequence as shown. In order to allow the puckering and flapping to interact, we utilized the two-dimensional function of eq 2 and the Hamiltonian of eq 14. Just the introduction of the kinetic energy expansions for g_{55} and g_{45} was sufficient to account for most of the unusual pattern of ring-puckering energy levels. The cross term in the potential surface ($cx_1^2x_2^2$) in eq 2 only played a minor role in perturbing the puckering levels. Thus, the reduced mass effects are the basis for most of the interaction. Figure 10 shows the two-dimensional potential energy surface,[24] which together with the kinetic energy expression, very nicely reproduces the 28 observed far-infrared frequencies with an average deviation of less than 2 cm^{-1} or about 1%. The tiny barrier to planarity of 35 cm^{-1} lies below the zero-point energy for these two modes. Hence, for all practical purposes the molecule is planar.

Phthalan $S_1(\pi,\pi^*)$ Electronic Excited State. Figure 11 shows a partial qualitative molecular orbital diagram correlating the orbital energy levels of benzene to phthalan or any of the other molecules in this group. The reduction of the benzene D_{6h} symmetry to C_{2v} in phthalan results in the splitting of the benzene bonding E_{1g} orbitals and the antibonding E_{2u} orbitals into A_2,B_2 pairs. Analysis of the ultraviolet absorption band types[25] shows that the $S_1(\pi,\pi^*)$ excited-state results from the
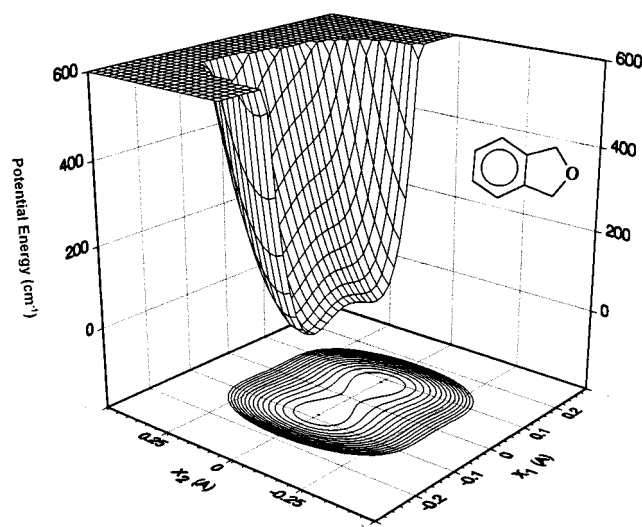
Figure 10. Potential energy surface for the ring-puckering (x_1) and ring-flapping of phthalan.
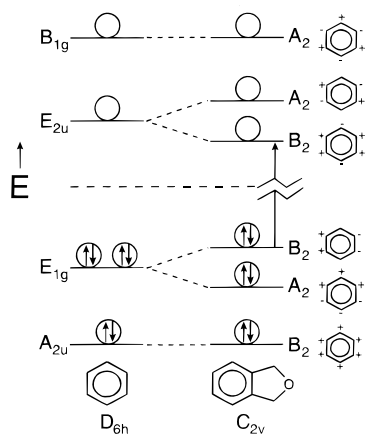

Figure 11. Molecular orbital diagram correlating to π orbitals of benzene to these of phthalan. The skeletal atoms of phthalan are assumed to be in the xz plane.
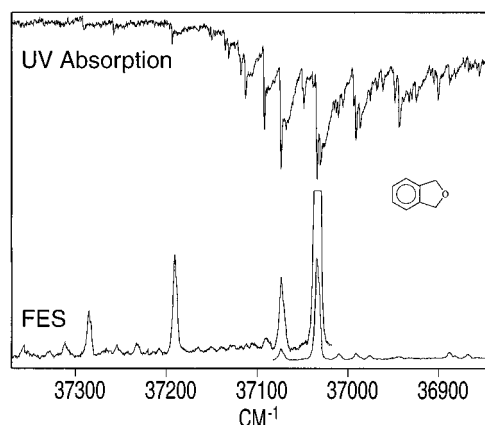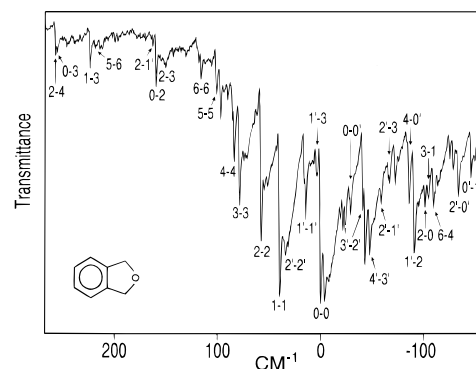

Figure 12. Fluorescence excitation and ultraviolet absorption spectra of phthalan.

$B_2 \rightarrow B_2$ transition as shown in Figure 11. The ordering of the orbital energies was also confirmed by ab initio calculations.[25]

Figure 12 shows the laser-induced fluorescence excitation spectrum (FES) of the jet-cooled phthalan and also the ultraviolet absorption spectrum of phthalan vapor at 25 °C. The pure electronic transition 0_0^0 is at 37 034.2 cm^{-1} in both spectra. Since the $S_1(\pi,\pi^*)$ state has A_1 symmetry resulting from the $B_2 \rightarrow B_2$ electronic transition, the vibronic ring-puckering energy
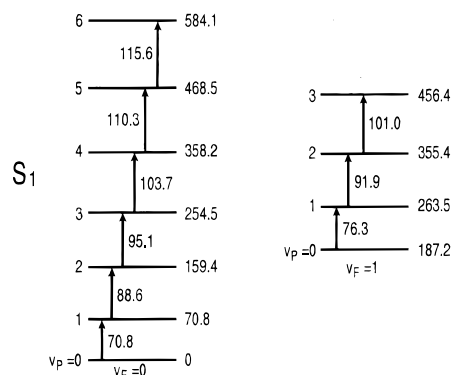

Figure 13. Ultraviolet absorption spectra of phthalan vapor near the electronic band origin. The ring-puckering transitions and labeled. Primes refer to the $\nu_F = 1$ state.

levels in this state have A_1 symmetry for $\nu_P =$ even and B_2 for $\nu_P =$ odd. Hence, the most intense transitions in the spectra (Figure 12) correspond to $\Delta\nu_P = 0, 2, 4$, etc. where there is no symmetry change between the vibrational levels. However, rather surprisingly, a large number of weak $\Delta\nu_P =$ odd transitions were also observed. This presumably results from the high anharmonicity of the ring-puckering vibration in both electronic states. Figure 13 shows an expanded region of the ultraviolet absorption spectrum near the band origin 0_0^0. Many of the bands are labeled by their ring-puckering quantum numbers. The primes refer to transitions to or from a ring-flapping excited state with $\nu_F = 1$. Some of these are shown in Figure 4. From the FES only ring-puckering levels up to $\nu_P = 3$ can be observed. However, the UV absorption spectra show transitions up to $\nu_P = 6$ since the higher puckering levels in S_0 are significantly populated and these have better transition moments to the higher levels than those from $\nu_P = 0$ (or $\nu_P = 1$ for warmer FES spectra). In addition, four of the ring-puckering levels in the $\nu_F = 1$ flapping states were determined from the spectra. Figure 14 shows the puckering levels for both the S_0 and $S_1(\pi,\pi^*)$ states for both $\nu_F = 0$ and $\nu_F = 1$ flapping states, and the changes in the electronic excited state can be seen to be quite large. The $\pi \rightarrow \pi^*$ transition to the S_1 state can be expected to reduce the rigidity of this bicyclic ring molecule, and this is reflected in the decrease in the ring-flapping frequency from 215.9 cm^{-1} in S_0 to 187.2 cm^{-1} in S_1. Surprisingly, however, the puckering of the five-membered ring takes on a more rigid potential energy function. Figure 15 shows the two-dimensional potential energy surface for the $S_1(\pi,\pi^*)$ state which fits the experimental data very well. This has the form

$$V \text{ (cm}^{-1}) = 7.96 \times 10^5 x_1^4 + 4.09 \times 10^3 x_2^2 + 1.44 \times 10^5 x_1^2 x_2^2 \quad (15)$$

Thus, the function is essentially pure quartic in nature (no x_1^2 term). It has a cross term ($x_1^2 x_2^2$) which is 3.5 times higher than that for the S_0 ground state, indicating that here the potential energy interactions have become much more significant. The kinetic energy interactions, just as for the ground state, are also large. The function in eq 15, unlike the S_0 function, has no barrier to planarity. Moreover, along the puckering coordinate the potential energy function is somewhat stiffer. This is shown in Figure 16 where the ring-puckering potential energies (along $x_2 = 0$) for the S_0 and S_1 states are compared. The energy level separations are also shown for the excited state. There is no obvious explanation why the ring-puckering potential energy function should become more rigid in S_1 and why the small barrier to planarity should disappear.

Feature Article

J. Phys. Chem. A, Vol. 104, No. 33, 2000 **7721**

Figure 14. Ring-puckering (v_P) quantum levels of phthalan for the ring-flapping $v_F = 0$ and 1 states for both the electronic ground (S_0) and excited states (S_1).
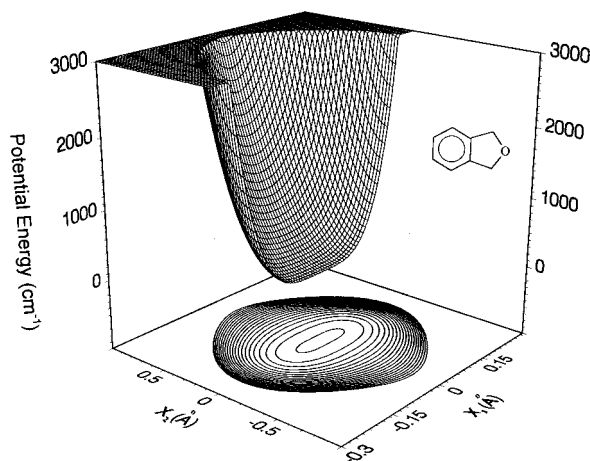

Figure 15. Potential energy surface for phthalan in its $S_1(\pi,\pi^*)$ electronic excited state in terms of its ring-puckering (x_1) and ring-flapping (x_2) coordinates.

Ab initio calculations have been carried out for both the S_0 and S_1 states of phthalan and the other molecules in this family of compounds. These will be discussed later.

1,3-Benzodioxole in the S_0 Ground State. This molecule is of special interest since it is expected to show the anomeric effect, which can occur when a $-O-CH_2-O-$ configuration is present in a molecule. Previously we have studied the far-infrared and Raman spectra of 1,3-dioxole,[34] $OCH_2OCH=CH$, and showed that its barrier to planarity is 325 cm^{-1}. This is believed to arise from a desire of the molecule to get better overlap between a $\sigma^*(C-O)$ orbital and the lone-pair orbital on the other oxygen atom. For 1,3-benzodioxole we wished to
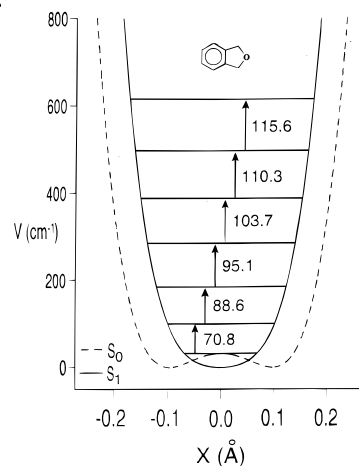

Figure 16. Ring-puckering potential energy curves for the phthalan $S_1(\pi,\pi^*)$ excited state. The flapping coordinate x_2 in Figures 15 (eq 15) and 10 is set equal to zero.
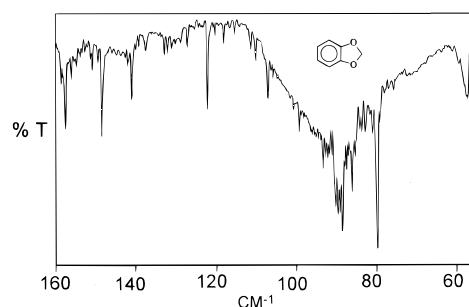

Figure 17. Far-infrared spectra of 0.5 Torr of 1,3-benzodioxole with a path length of 20 m.
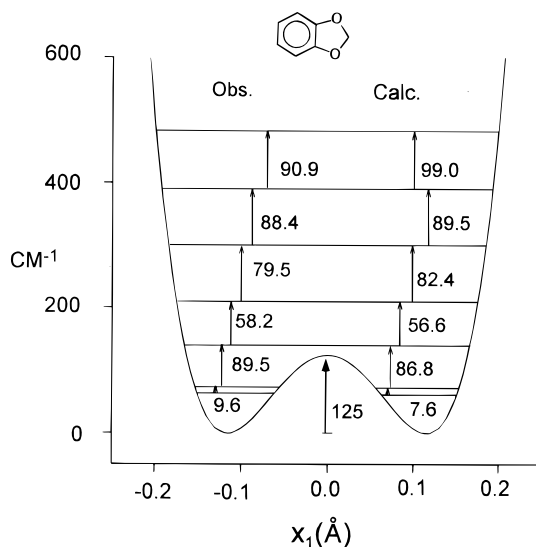

Figure 18. One-dimensional ring-puckering potential energy function calculated for 1,3-benzodioxole.

investigate what the influence of the benzene ring has on the anomeric effect and then determine what effect the electronic $\pi \rightarrow \pi^*$ transition has on this. Figure 17 shows the far-infrared spectrum of this molecule.[26] Raman spectra showing $\Delta v_P = 2$ transitions of the vapor confirm the far-infrared assignments. The data can be fit moderately well with a one-dimensional potential function (Figure 18), but the deviations between observed and calculated values clearly shows the need to consider interactions with the ring flapping. Thus, the ring-puckering energy levels for both the flapping $v_F = 0$ and 1 states
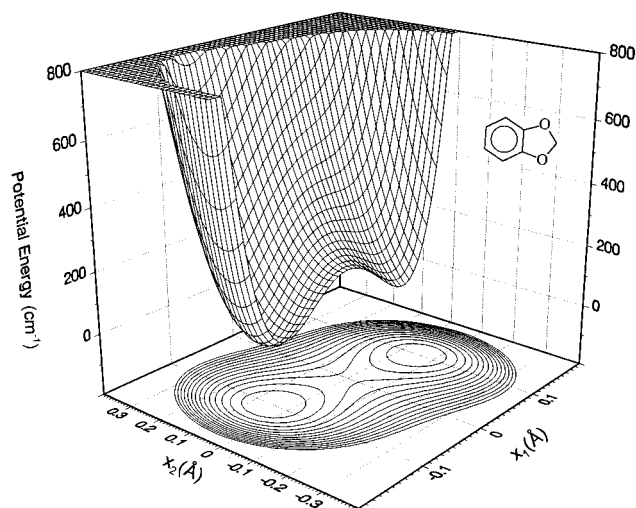
Figure 19. Potential energy surface for the ring-puckering (x_1) and ring-flapping (x_2) vibrations of 1,3-benzodioxole in the S_0 state.
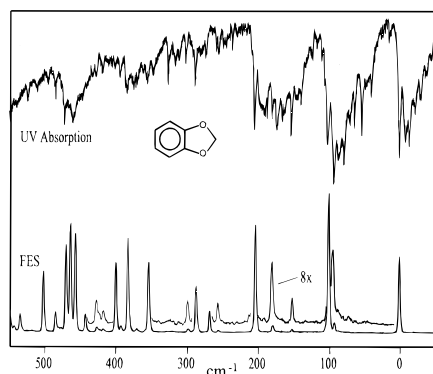

Figure 20. Fluorescence excitation and electronic absorption spectra of 1,3-benzodioxole.

Figure 21. Ultraviolet absorption spectra of 1,3-benzodioxole near the electronic band origin.

were utilized in a two-dimensional potential energy calculation. (These will be compared to the excited state levels later.) The kinetic energy expressions $g_{44}(x_1,x_2)$, $g_{55}(x_1,x_2)$, and $g_{45}(x_1,x_2)$ were calculated and used for the determination of the two-dimensional potential energy surface shown in Figure 19. This has a barrier to planarity of 164 cm^{-1} and puckering and flapping angles of $\pm24°$ and $\mp3°$, respectively. If the flapping angle is forced to be zero, only a slightly worse frequency fit results. Hence, the experimental data are only sufficient to show that the flapping angle is $3° \pm 3°$. However, ab initio calculations predict puckering and flapping angles of 24.2° and 2.6° along with a barrier of 171 cm^{-1}, in remarkable agreement with the experiment.

The 164 cm^{-1} barrier for 1,3-benzodioxole clearly arises from the anomeric effect as there are no $-CH_2-CH_2-$ torsional forces present to produce a nonplanar five-membered ring. However, the barrier is only about half that of 1,3-dioxole, which is similar except that it possesses no benzene ring. Hence, there is a strong indication that the anomeric effect is suppressed by the presence of the benzene ring.

1,3-Benzodioxole in the $S_1(\pi,\pi^*)$ State. The molecular orbital diagram in Figure 11 is also applicable to 1,3-benzodioxole. Because this molecule is puckered in both its ground and excited states, the molecular symmetry is C_s rather than C_{2v}. Nevertheless, the C_{2v} selection rules hold for the most part.

Figure 20 shows the fluorescence excitation spectrum and the ultraviolet absorption spectrum of the molecule.[27] The electronic band origin is at 34 789.8 cm^{-1}. These spectra were
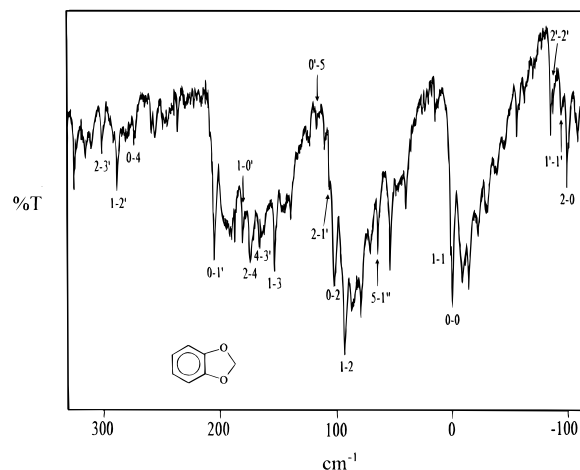
quite difficult to assign, especially before we realized that the 0_0^0 pure electronic band tends to obscure the $1 \rightarrow 1$ transition for the puckering which is only 1.4 cm^{-1} higher. This was resolved in high-resolution absorption spectra, however. The assignment was also complicated by the fact that many transitions to flapping excited levels (labeled with primes in the figures) in the $S_1(\pi,\pi^*)$ electronic excited state are among the most intense in the spectra. Figure 21 shows the UV absorption spectrum near the band origin along with the assignments for many of the transitions. The $1 \rightarrow 1$ transition can be barely seen in this figure. The intensity of the $0 \rightarrow 1'$ transition, which also corresponds to the most intense band in the FES, should be noted. As can be seen, most of the transitions are v_P = even to even or odd to odd ($A_1 \rightarrow A_1$ or $B_2 \rightarrow B_2$) when the flapping vibration is not involved. In the flapping excited state, which has B_2 symmetry; however, the v_P = even levels become B_2 and the odd ones become A_1, reversing their symmetries. Hence, the $0 \rightarrow 1'$ and the $1 \rightarrow 2'$ are now $A_1 \rightarrow A_1$ and $B_2 \rightarrow B_2$, respectively, for example. The $1 \rightarrow 2$ band intensity for an odd $\rightarrow$ even transition is surprisingly large, but both these levels are below the barrier so this is actually an $A' \rightarrow A'$ transition for a C_s molecule. Figure 22 presents the ring-puckering energy levels in several flapping states (v_F = 0, 1, 2) for both the S_0 and S_1 electronic states. The 0−1 splitting from S_0 to S_1 can be seen to increase by 1.3 cm^{-1} and explains why the $1 \rightarrow 1$ transitions is nearly coincident with the $0 \rightarrow 0$. The ring-flapping frequency drops from 267.2 to 189.5 cm^{-1}, and this reflects the fact that the electronic transition weakens the π bonding allowing the five-membered ring to flap more readily relative to the benzene ring. This frequency change of 77.7 cm^{-1} is large when compared to that in phthalan (28.7 cm^{-1}) and can be accounted for by the decreased interaction between the oxygen nonbonded orbitals and the benzene ring in the S_1 state. This will be discussed in more detail below.

Figure 23 shows the two-dimensional potential energy surface determined for 1,3-benzodioxole in terms of the puckering (x_1) and flapping (x_2) coordinates. The barrier to planarity is 264 cm^{-1} and the dihedral angle of puckering is 22°. Within experimental error, the flapping angle is 0°.

As described above, the somewhat suppressed anomeric effect produces a barrier of 164 cm^{-1} for 1,3-benzodioxole in its electronic ground state. This barrier increases upon $\pi \rightarrow \pi^*$ electronic excitation to 264 cm^{-1}, apparently because the anomeric effect is less suppressed in S_1. A comparison of the potential energy along the ring-puckering coordinate is shown
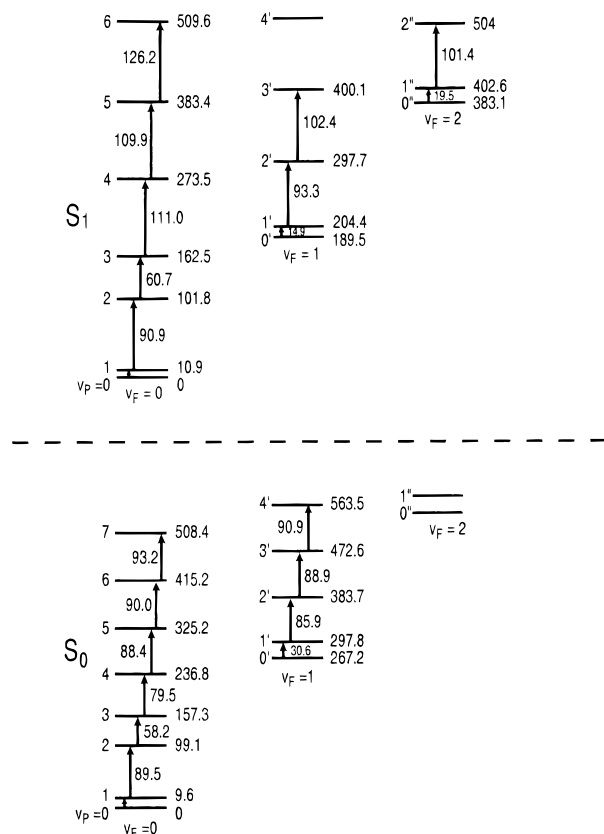
Feature Article

J. Phys. Chem. A, Vol. 104, No. 33, 2000 **7723**

Figure 22. Ring-puckering energy levels for 1,3-benzodioxole in different flapping states for S_0 and S_1.
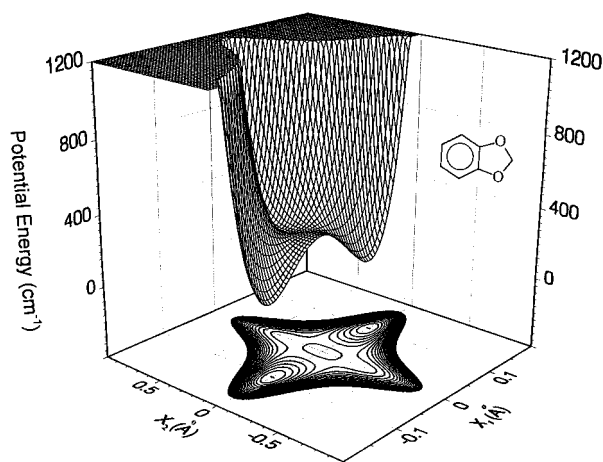

Figure 23. Potential energy surface for 1,3-benzodioxole in its S_1-(π,π^*) electronic excited state. x_1 = ring-puckering; x_2 = ring-flapping.

Figure 24. Comparison of ring-puckering potential energy (with $x_2 = 0$) for the ground and excited states of 1,3-benzodioxole.

Figure 25. Benzene ring p_π orbitals and orbitals involved in the anomeric effect for planar and puckered forms of 1,3-benzodioxole.

Figure 26. Far-infrared spectrum of coumaran vapor.

for both electronic states in Figure 24. Figure 25 shows the molecule in both its planar and puckered forms along with the p_π orbitals on the benzene ring, one of the oxygen nonbonding orbitals, and one $\sigma^*(C-O)$ orbital. When the molecule is planar, overlap between the oxygen p orbital and the benzene π system is maximized but the p$-\sigma^*$ interaction is not possible. Upon puckering, the benzene$-$p(O) interaction is decreased while the p$-\sigma^*$ interaction is increased. In the S_0 state the p_π orbitals compete strongly for interaction with p(O), thus suppressing the anomeric effect and allowing less puckering. In the $S_1(\pi,\pi^*)$ excited state the benzene ring π bonding is reduced as is the interaction between the p_π and p(O) orbitals. Hence, the anomeric effect is less suppressed and the ring can pucker further.
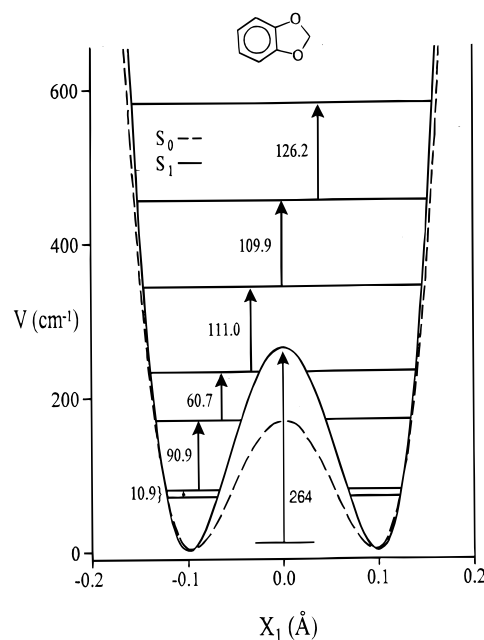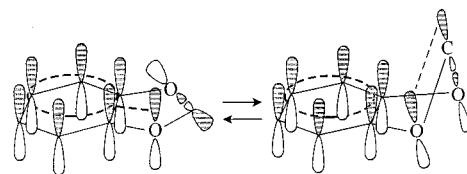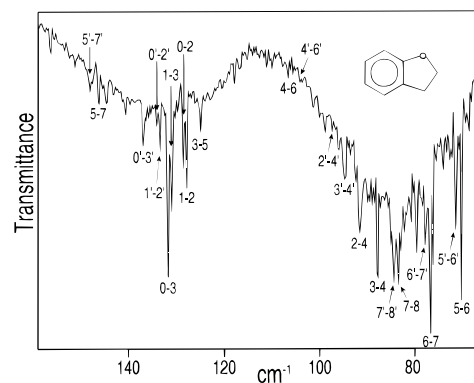
Coumaran in Its Electronic Ground State. The far-infrared spectrum of coumaran is shown in Figure 26 along with the assignment of many of the ring-puckering transitions.[28] The spectrum is fairly noisy since the sample vapor pressure is less than 1 Torr. Nevertheless, in addition to the usual $\Delta v_P = 1$ transitions, many weaker $\Delta v_P = 2$ and 3 transitions as well as transitions involving the $v_F = 1$ flapping excited state (labeled with primes) can be observed. These can be fit quite well with just a one-dimensional potential energy function which is shown in Figure 27. This has a barrier to planarity of 279 cm^{-1} and the energy minima at $x = \pm0.14$ Å correspond to dihedral angles of $\pm30°$. The data also define the energy levels very well for the flapping excited state ($v_F = 1$) and these are shown in Figure 28. The energy spacing changes from $v_F = 0$ to 1 are substantial and arise from the interactions between the puckering and flapping motions. This has also been accounted for with a two-

TABLE 1: Comparison of Experimental and ab Initio Results for Molecules in the Indan Family

| | ground state | | | | $S_1(\pi,\pi^*)$ excited state | | | | | |
| | barrier | | dihedral angles (cm^{-1})^a | | barrier | | dihedral angles | | v_0^0 (cm^{-1}) | |
molecule	expt	ab initio^b	expt	ab initio^b	expt	ab initio^c	expt	ab initio^c	expt	ab initio
phthalan	35	91	0	23°	0	0	0	0	37 034	46 635
1,3-benzodioxole	164	171	24°, 3°	25°, 3°	264	369	24°	29°	34 790	36 986
coumaran	279	258	30°	27°	?		?		34 870	
indan	434^e	662	30°	32°	~300		~25°		36 904	

^{a} Puckering angle except for 1,3-benzodioxole for which the flapping angle is also given. ^{b} Using MP2/6-31G* basis set. ^{c} Using CIS/6-311+G(2s,p)//CIS/6-31+G* basis set. ^{d} Value of energy minimum; the lowest puckering level is only slightly below the calculated barrier. ^{e} Value calculated from microwave study, ref 32.
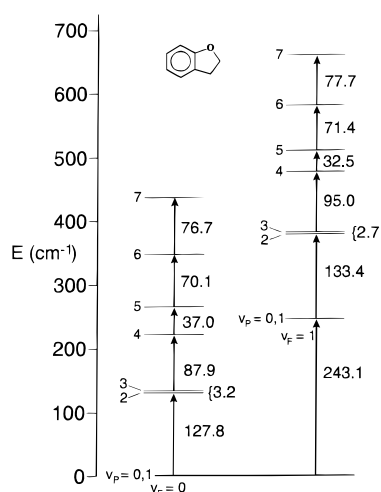

Figure 27. Energy levels for the ring-puckering in the $v_F = 0$ and 1 flapping states of coumaran.
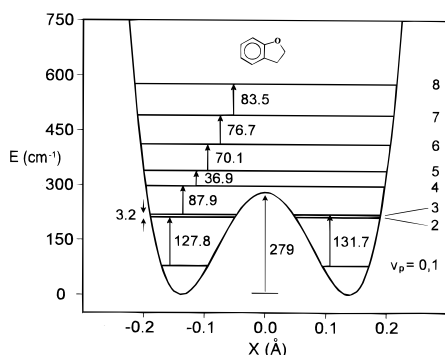

Figure 28. Potential energy function and observed transitions for the ring-puckering of coumaran.

dimensional potential energy surface which has a very similar barrier of 275 cm^{-1}.

The barrier to inversion of coumaran is considerably higher than that for 2,3-dihydrofuran[25] (83 cm^{-1}). This is expected since the angle strain, which favors a planar structure, is lower for the coumaran molecule.

Ab Initio Calculations. For the electronic ground state the ab initio calculations[25–27,33] are in remarkably good agreement with the experimental results determined here and this is shown in Table 1. For phthalan, both experiment (35 cm^{-1}) and calculation (91 cm^{-1}) predict only a tiny blip of a barrier. For 1,3-benzodioxole and coumaran the differences between experimental and calculated barriers are only 7 and 21 cm^{-1}, respectively (0.02 and 0.06 kcal/mol). For indan the microwave result of 434 cm^{-1} for the barrier is well below the 665 cm^{-1} value from the ab initio computation. However, we believe it is quite likely that the experimental number will be higher when
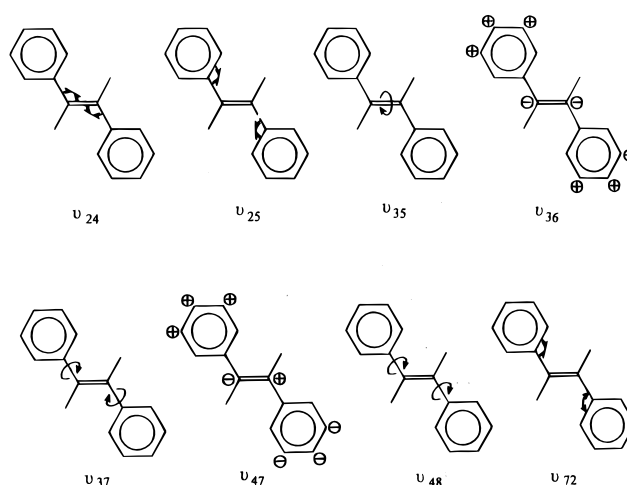

Figure 29. Low-frequency vibrations of *trans*-stilbene.

we complete the far-infrared and dispersed fluorescence analysis of the S_0 ground state.

Ab initio calculations for electronic excited states are considerably more challenging. Even predicting the frequency of the electronic transition is far from routine. Calculations at the CIS/6-311+G(2s,p)//CIS/6-31+G* level are moderately good, predicting the electronic transition to be at 36 986 cm^{-1} (vs 34 790 cm^{-1} experimental) and calculating the barrier to planarity of 369 cm^{-1} (vs 264 cm^{-1} experimental) for 1,3-benzodioxole. Results for the other molecules are also shown in Table 1.

B. *trans*-Stilbene in Its Ground and $S_1(\pi,\pi^*)$ Excited States. The *trans*–*cis* photoisomerization of stilbene has been of interest to experimental and theoretical chemists for many years.[36,37] In the electronic ground state there is a reported barrier to isomerization of 48.3 kcal/mol.[37] Hence, the internal rotation about the C=C bond does not occur in S_0. The photoisomerization in the $S_1(\pi,\pi^*)$ excited state can take place since the potential energy minimum for the internal rotation corresponds to a twisted (perpendicular) configuration and a relatively small barrier exists between the *trans* and twisted forms. In 1992 Banares, Heikal, and Zewail[38] studied the dynamics of the photoisomerization and concluded that the *trans*-twist barrier is about 1200 cm^{-1}.

The analyses of both the S_0 and $S_1(\pi,\pi^*)$ states of *trans*-stilbene are complicated by the fact that this molecule has eight vibrations with frequencies below 300 cm^{-1}. These are shown in Figure 29. For many years there was considerable debate about the assignments for *trans*-stilbene vapor for which only dispersed fluorescence data were available for the electronic ground state. However, Haller, Chiang, and Laane[39] succeeded in recording the vapor-phase Raman spectrum of this molecule at 330 °C. The low-frequency region of the spectrum with perpendicular and parallel polarizations is shown in Figure 30.
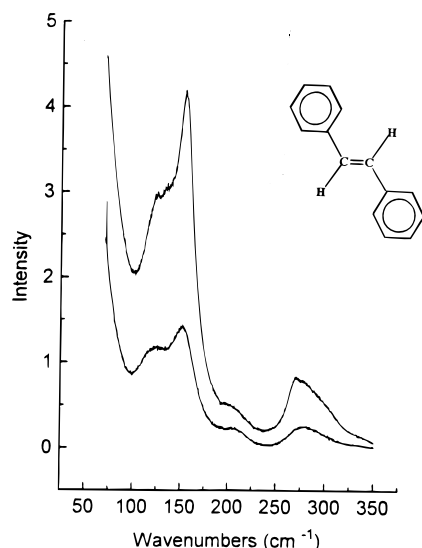
Feature Article

J. Phys. Chem. A, Vol. 104, No. 33, 2000 **7725**

Figure 30. Low-frequency Raman spectrum of *trans*-stilbene vapor at 330 °C. The upper curve is the parallel polarized spectrum, the lower is the perpendicular polarized spectrum.
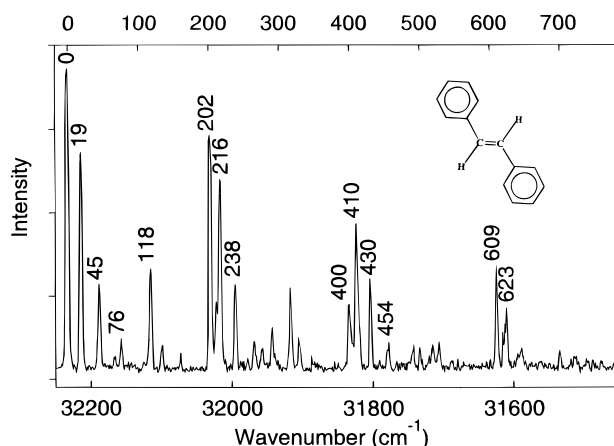

Figure 31. Dispersed fluorescence spectra of the 0_0^0 band of *trans*-stilbene.

Figure 32. Fluorescence excitation spectra of jet-cooled *trans*-stilbene.

Figure 33. Vibrational energy spacings for four low-frequency vibrations of *trans*-stilbene in its ground and excited states.

The two polarized bands at 273 and 152 cm^{-1} must clearly be the two A$_g$ modes. Somewhat surprisingly, these are not observed in the dispersed fluorescence spectrum (Figure 31). The weaker depolarized bands at 211 and 118 cm^{-1}, which do have dispersed fluorescence counterparts, correspond to the two B$_g$ modes. The dispersed fluorescence spectrum in Figure 31 was recorded[36] from the 0_0^0 excitation band at 32 232 cm^{-1}. Other dispersed spectra were recorded from excitation bands at 39, 70, 83, and 95 cm^{-1}. Figure 32 shows the laser-induced fluorescence excitation spectrum of the jet-cooled *trans*-stilbene.[36] All but the first of these excitation bands used for the dispersed spectra originate from the vibrational ground state in S$_0$. The 39 cm^{-1} band originates from an excited phenyl torsion level which is only 9 cm^{-1} above the ground state. Even with jet-cooling, this level has a substantial molecular population. Because of symmetry factors, the 0_0^0 spectrum in Figure 31 shows transitions only to every other phenyl torsion level in S$_0$. Since the symmetry properties of the 9 cm^{-1} level are different from the those of the vibrational ground state, the dispersed spectrum from the 39 cm^{-1} excitation band shows transitions to the missing levels. Figure 33 shows the energy spacings for both the S$_0$ and S$_1$ states. In Figure 31 the bands at 19, 45, and 76 cm^{-1} result from transitions to the (4,5), (8,9), and (12,13) quantum states of the phenyl torsions. Because both
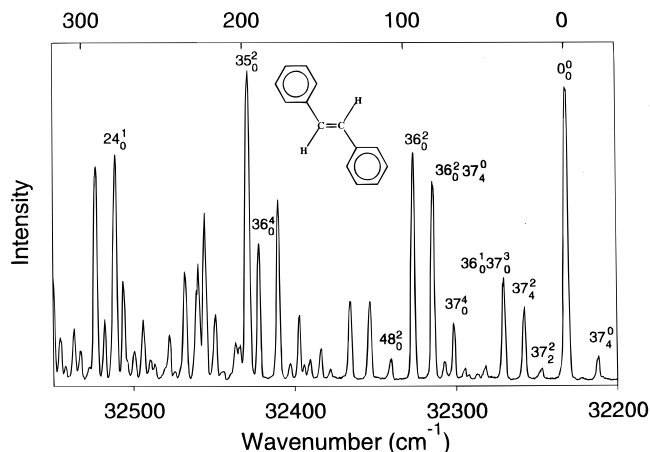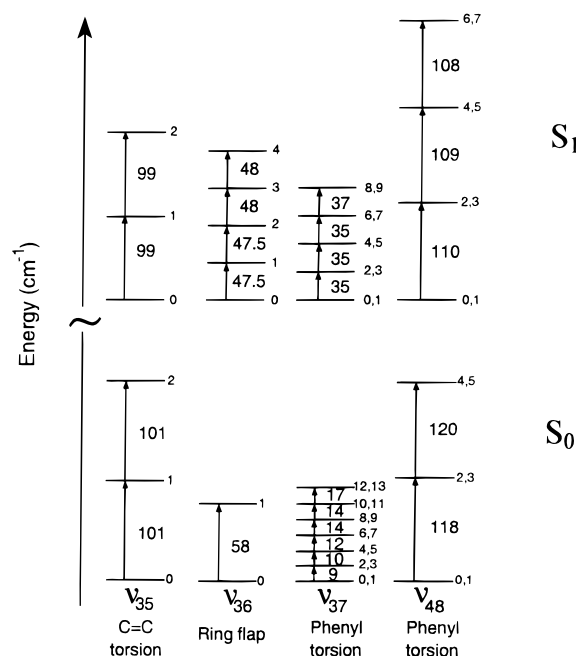
phenyl torsions are doubly degenerate, each energy level for each of the vibrations is actually 4-fold degenerate. Some previous analyses of the *trans*-stilbene spectra had not recognized this degeneracy.

Table 2 summarizes the vibrational frequency assignments for both the S$_0$ and S$_1$ (π,π^*) states for *trans*-stilbene and also for 4-methoxy-*trans*-stilbene,[40] which we have analyzed in a similar manner. Of particular interest are the phenyl torsions

TABLE 2: Vibrational Assignments (cm^{-1}) for the Low-Frequency Vibrations of *trans*-Stilbene in Its S$_0$ and S$_1(\pi,\pi^*)$ States

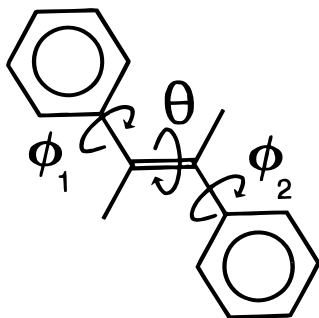| C_2h	approximate description	*trans*-stilbene		4-methoxy-*trans*-stilbene	
		S$_0$	S$_1(\pi,\pi^*)$	S$_0$	S$_1(\pi,\pi^*)$
A$_g$	ν_{24} C$_e$—Ph bend	273	280	234	279
	ν_{25} phenyl wag (i.p.)	152	(150)^a	144	(140)^a
A$_u$	ν_{35} C=C torsion	101	99	86	85.5
	ν_{36} phenyl flap	58	47.5	59	46
	ν_{37} phenyl torsion	9	35	8	28
B$_g$	ν_{47} phenyl flap	211	(200)^a	179	(170)^a
	ν_{48} phenyl torsion	118	110	123	109
B$_u$	ν_{72} phenyl wag (i.p.)	76	(70)^a	68	(65)^a

^{a} Estimate.

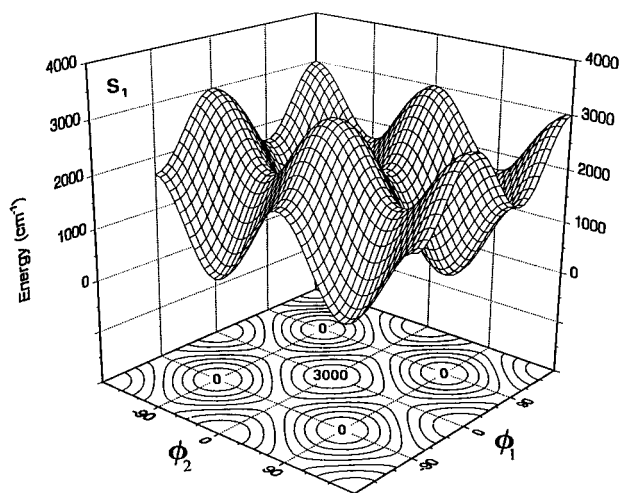**Figure 34.** Torsional coordinates for *trans*-stilbene.

Figure 35. Potential energy surface for the phenyl torsions of *trans*-stilbene in its $S_1(\pi,\pi^*)$ state.

(v_{37} and v_{48}) and the torsion about the double bond (v_{35}), which for the most part governs the photoisomerization. As mentioned above and shown in Figure 33, many of the quantum states for the phenyl torsions have been mapped out and these are discussed below. The torsion about the C=C bond (A_u symmetry) is observed as a series of overtones 202, 400/410 doublet, 609 cm^{-1}, etc. in the dispersed spectra (Figure 31) for the S_0 ground state. Hence, the fundamental band is at 101 cm^{-1}, and this is compatible with the 48.3 kcal/mol barrier previously reported for the ground state.[37]

Figure 34 defines the ϕ_1 and ϕ_2 coordinates used to represent the phenyl torsions and θ which represents the internal rotation about the C=C bond. The phenyl torsions were treated as a two-dimensional problem and a computer program was written to calculate the coordinate dependent kinetic energy (reciprocal reduced mass) function in terms of ϕ_1 and ϕ_2. This was then utilized in the potential energy computation with

$$V(\phi_1,\phi_2) = {}^1/_2 V_2(2 + \cos 2\phi_1 + \cos 2\phi_2) + V_{12} \cos 2\phi_1 \cos 2\phi_2 + V'_{12} \sin 2\phi_1 \sin 2\phi_2 \quad (16)$$

A separate computer program was written to determine the energy levels for this potential energy surface and to optimize the potential energy parameters V_2, V_{12}, and V'_{12}. For the S_0 ground state the values determined were $V_2 = 1550$ cm^{-1}, $V_{12} = 337.5$ cm^{-1}, and $V'_{12} = 402.5$ cm^{-1}. For S_1 these were found to be $V_2 = 1500$ cm^{-1}, $V_{12} = -85$ cm^{-1} and $V'_{12} = -55$ cm^{-1}. Figure 35 shows the potential energy surface for the $S_1(\pi,\pi^*)$ excited state. The coordinates are defined so that at $\phi_1 = \phi_2 = 0$ both phenyl groups are perpendicular to the $-C-C=C-C-$ skeleton. Here the potential energy has its maximum value of
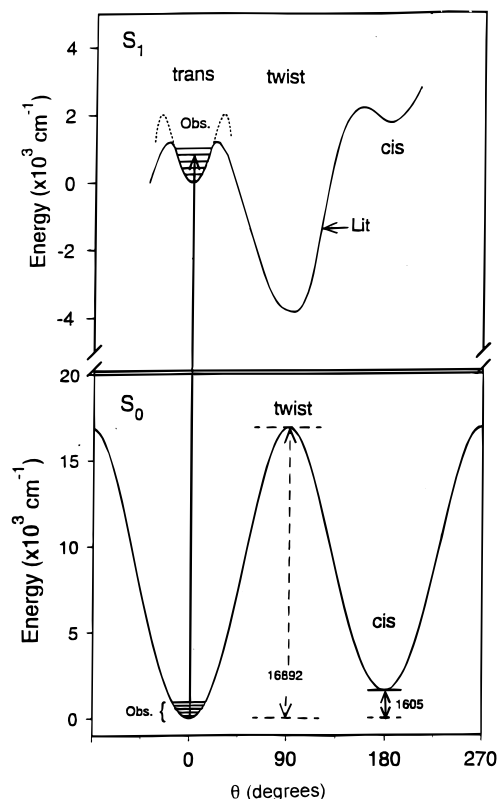

Figure 36. Potential energy function for the internal rotation of *trans*-stilbene about the C=C bond. $\theta = 0°$ corresponds to the *trans* isomer.

3000 cm^{-1} ($2V_2$). There are four equivalent energy minima at $\phi_1 = \pm90°$ and $\phi_2 = \pm90°$, where the entire skeleton of the molecule lies in a plane. The barrier to rotating a single phenyl ring is 1670 cm^{-1}. The S_0 potential energy surface is qualitatively similar with a barrier at $\phi_1 = \phi_2 = 0$ of 3100 cm^{-1}. However, the barrier to rotating a single phenyl group is only 875 cm^{-1}. Both the S_0 and S_1 surfaces require three potential energy parameters, and these do an excellent job of fitting all of the observed energy spacings. Even the large difference (9 cm^{-1} vs 118 cm^{-1}) between the out-of-phase and in-phase phenyl torsions is very nicely reproduced.

In order to represent the internal rotation about the C=C double bond, a computer program was written to calculate the coordinate dependent kinetic energy function. For the S_0 ground state this was used to calculate the potential energy parameters for the one-dimensional potential function

$$V(\theta) = {}^1/_2 V_1(1 - \cos \theta) + {}^1/_2 V_2(1 - \cos 2\theta) + {}^1/_2 V_4(1 - \cos 4\theta) \quad (17)$$

where $\theta = 0°$ and 180° correspond to the *trans* and *cis* isomers, respectively, where V_1 is the energy difference between the *trans* and *cis* forms, where V_2 almost entirely determines the barrier, and where V_4 is a shaping parameter. When the literature values[35] $V_1 = 1605$ cm (4.6 kcal/mol) and $V_2 = 16\,892$ cm^{-1} (48.3 kcal/mol) are used, excellent frequency agreement between the experimental and calculated data is obtained using $V_4 = -900$ cm^{-1}. Since our data is confined to the bottom region of a potential energy function which has a very high barrier, the calculation of V_2 by extrapolation does not give a very accurate value (15 000 ± 3000 cm^{-1}). However, the data is totally consistent with the literature values. The lower half of Figure 36 shows the potential energy curve for the S_0 state.

Feature Article

J. Phys. Chem. A, Vol. 104, No. 33, 2000 **7727**

The C=C torsion data for the $S_1(\pi,\pi^*)$ state are only observed for the *trans* conformation (due to the Franck−Condon Principle) although the energy minimum for this electronic state occurs for the twist form ($\theta = 90°$). Figure 36 (top section) shows the qualitative potential energy curve estimated in the literature. The figure also shows the vibronic energy levels observed within the *trans* potential well. No fluorescence excitation spectra can be observed going to levels in the twist well. In addition, the *cis* well is apparently too shallow to allow transitions originating from the S_0 state of *cis*-stilbene. Consequently, the fluorescence data allow only the shape of the *trans* well to be calculated, and this is shown as the dotted line in Figure 36. This can be represented by several different forms[36] for the potential energy function including

$$V(\theta) = {}^1\!/_2 V_1(1 - \cos\theta) + {}^1\!/_2 V_2(1 - \cos 2\theta) +$$
$$ {}^1\!/_2 V_4(1 - \cos 4\theta) + {}^1\!/_2 V_8(1 - \cos 8\theta) \quad (18)$$

Here, V_1 represents the *trans/cis* energy difference and V_2 primarily determines the depth of the twist well. We have no experimental data for either of these, and their values have little effect on the vibronic levels in the *trans* well. V_4 primarily determines the *trans* → twist barrier while V_8 is a minor shaping term. Analysis of the experimental data, which extend 1230 cm^{-1} above the *trans* well minimum, shows that the *trans* → twist barrier is somewhat higher than the 1200 cm^{-1} estimated from the dynamics data.[38]

C. Cyclic Ketones in Their $S_1(n,\pi^*)$ States. The lowest lying electronic state for many ketones results from the n to π^* transition producing the $S_1(n,\pi^*)$ state in which the bond order of the C=O bond has been reduced to 1.5. In this electronic state, a carbonyl compound typically distorts from a planar to a pyramidal configuration about the carbonyl carbon atom. This was predicted for formaldehyde in 1953 by Walsh[41] and verified spectroscopically by Brand in 1956.[42] The $S_1(n,\pi^*)$ state of acetaldehyde has been studied by fluorescence and absorption methods since 1954 as a prototype of larger carbonyl compounds.[43−45] However, its electronic absorption spectrum is complex and ill-resolved, and little agreement existed on the interpretation. Only recently, with the vibrational and rotational cooling obtained in a supersonic jet, did it become possible to make accurate assignments.[46−48] We have recently recorded and analyzed the fluorescence excitation spectra (FES) for several cyclic ketones in a supersonic jet including 2-cyclopenten-1-one (2CP), 3-cyclopenten-1-one (3CP), cyclopentanone (CP), cyclobutanone (CB), bicyclo[3.1.0]hexan-3-one (BCHO), tetrahydorfuran-3-one (THFO), and tetrahydrothiophen-3-one (THTP), and these results will be discussed here. The electronic absorption spectra of 2CP,[49] 3CP,[49] CP,[50] and CB[51] at room temperature had previously been reported, but without jet cooling to simplify the spectra it was difficult to assign the spectra correctly. The fluorescence spectra for these molecules are considerably weaker than the $\pi \to \pi^*$ transitions discussed above for the indan family or *trans*-stilbene. The pure electronic transition is strictly forbidden for 3CP and CB, for example, which have C_{2v} symmetry and for which the electronic transition is to an A_2 excited electronic state. Transitions to vibronic levels for B_2 vibrations such as the carbonyl wagging or ring-puckering, however, become symmetry allowed.
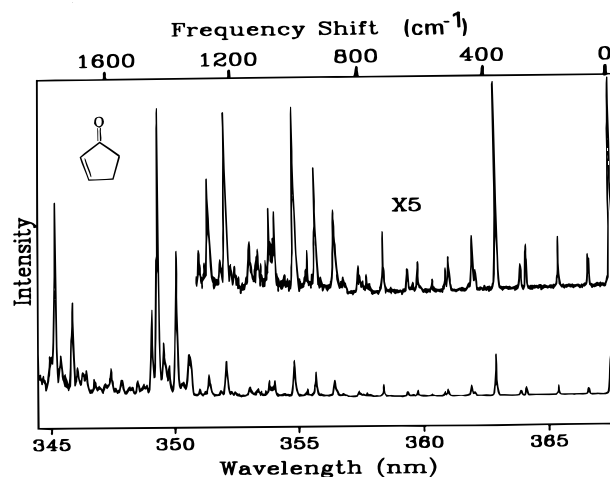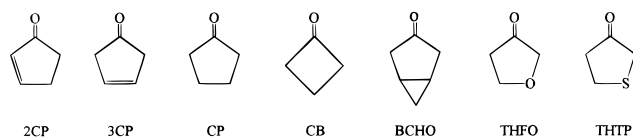

Figure 37. Fluorescence excitation spectrum of jet-cooled 2CP.

TABLE 3: Vibrational Frequencies (cm^{-1}) for the Ground and Excited $S_1(n,\pi^*)$ States of 2-cyclopenten-1-one

approximate description	ground	excited
ν_5 C=O stretch	1748	1357
ν_6 C=C stretch	1599	1418
ν_{13} ring mode	1094	1037
ν_{14} ring mode	999	974
ν_{15} ring mode	912	906
ν_{16} ring mode	822	849
ν_{17} ring mode	753	746
ν_{18} ring mode	630	587
ν_{19} C=O def (‖)	464	348
ν_{26} α-CH bend	750	768
ν_{28} C=O def (⊥)	537	422
ν_{29} C=C twist	287	274
ν_{30} ring-puckering	94	67

2-Cyclopenten-1-one (2CP). Figure 37 shows the low-resolution FES of 2CP.[52] The spectra of the two deuterated species were also recorded. The electronic origin was observed at 27 210 cm^{-1}. In comparison to the other cyclic ketones, which will be considered later, the 2CP frequency is considerably lower. This is the expected result from the conjugation between the C=O and C=C groups which results in a lower energy π^* orbital. The electronic origin for 2CP is also extremely intense in contrast to the $S_1(n,\pi^*)$ origins of the other more symmetric molecules without conjugation.

The frequencies of the relevant fundamental vibrations determined for the electronic ground state[53] and S_1 excited state[52] are given in Table 3. Thirteen of the 30 S_1 excited state vibrational frequencies have been determined from the fluorescence excitation spectrum. For the higher frequency vibrations our FES assignments agree well (± 10 cm^{-1}) with the absorption study of Gordon and Orr.[49] However, we disagree on the assignments involving the ring-puckering (ν_{30}), ring-twisting (ν_{29}), and carbonyl out-of-plane (ν_{28}) wag, for reasons discussed elsewhere.[52]

The FES of 2CP shows ring- puckering bands at 67, 158, 256, and 360 cm^{-1} and the ring-twisting band at 274 cm^{-1}. Figure 38 compares the ring-puckering data for the ground and excited electronic states for 2CP and its d_1 and d_2 isotopomers. As will be seen, the ring-puckering series of bands can be fit nicely with a one-dimensional potential energy function. The C=O in-plane (ν_{19}) and out-of-plane (ν_{28}) wags occur at 348 and 422 cm^{-1}, with both values considerably lower in frequency than in the electronic ground state reflecting the decrease in π character of the C=O bond. For 2CP sufficient conjugation is retained in the $S_1(n,\pi^*)$ state that the carbonyl group remains
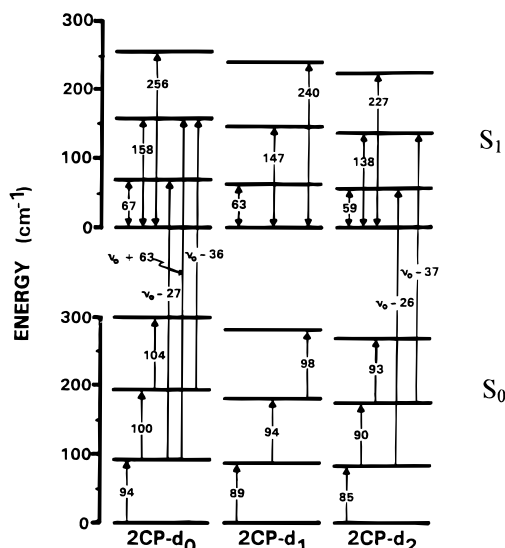
2CP   3CP   CP   CB   BCHO   THFO   THTP

7728 *J. Phys. Chem. A, Vol. 104, No. 33, 2000*

Laane

Figure 38. Energy level diagram for the ring-puckering vibrations of 2CP-d_0, 2CP-d_1, and 2CP-d_2 in the ground and $S_1(n,\pi^*)$ excited electronic states.
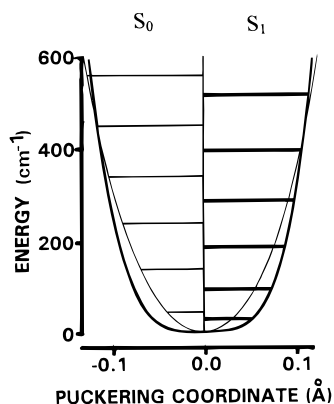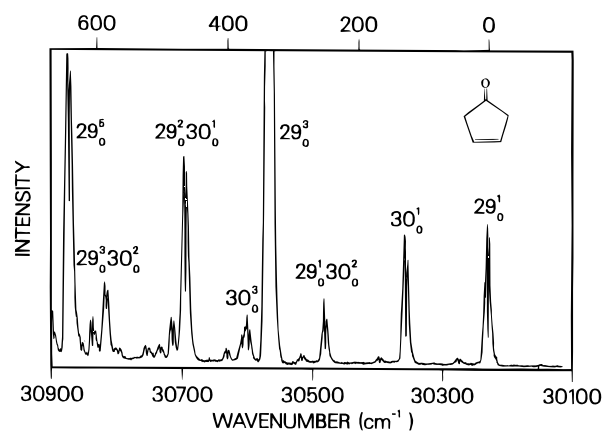

Figure 39. Potential energy function and energy levels for the ring-puckering vibration of 2CP in the ground (thin lines) and $S_1(n,\pi^*)$ excited (thick lines) electronic states.

in the plane of the planar ring system. For the other cyclic ketones to be discussed, this is not the case.

The intense bands at 1357 and 1418 cm^{-1} for 2CP-d_0 are clearly due to the C═O and C═C stretches, respectively. These two vibrations are Franck–Condon active due to the increased bond lengths for both bonds. The large drop in frequency for both of these in the excited state reflects both the conjugation between the groups and also the decrease in π bonding character.

The potential energy for the ring-puckering vibration in both the ground and excited electronic states can be analyzed using eq 1 while the Hamiltonian is given by eq 12. Figure 39 compares the functions and puckering energy levels for both states. As expected, the electronic excitation to an antibonding orbital results in a less rigid ring system and lower frequencies for the puckering vibration. However, the molecule, along with its C═O group, remains planar in both electronic states.

3-Cyclopenten-1-one (3CP). Figure 40 shows a portion of the jet-cooled fluorescence excitation spectrum[54] of 3-cyclo-penten-1-one with its band origin at 30,238 cm^{-1}. Each transition from the electronic ground state to an odd quantum state of the C═O wag (ν_{29}) in the A$_2$ electronic excited state has B$_2$ vibrational symmetry (assuming the molecule to lie in the xz plane), but has A$_1$ vibrational symmetry for even quantum states of the wag. Thus, only transitions to the odd states can be

Figure 40. Fluorescence excitation spectra of 3-cyclopenten-1-one.

observed. These show up as type B bands arising from A$_2$ × B$_2$ = B$_1$ symmetry. The first three of these transitions are labeled in Figure 40. It should be noted that since the $v = 0$ and $v = 1$ levels in the S$_1$(n,π^*) state are near-degenerate from inversion doubling, the band origin lies very close to the 0 → 1 frequency. The other bands in the spectrum include many combinations of the C═O wag with the ring-puckering vibration and combinations of these with other fundamentals including the C═O stretch. Of particular note is the $3_0^1 29_0^4 30_0^1$ band at 32 211 cm^{-1}, shifted 1973 cm^{-1} from the band origin and 746 cm^{-1} from the C═O stretching (ν_3) value at 1227 cm^{-1}. The 746 cm^{-1} value corresponds to the sum of the 0 → 4 wagging transition (ν_{29}) and the ring-puckering (ν_{30}) frequency of 127 cm^{-1}. This shows the 0 → 4 spacing to be 619 cm^{-1}, which is 20 cm^{-1} less than the 0 → 5 spacing.

In order to analyze the C═O wagging vibration in the electronic excited state, we have utilized our computer programs, described above, for calculating the reduced masses and energy levels for the Hamiltonian given in eq 12 and the potential energy function given by eq 1. Here x is used for the C═O wagging coordinate given in terms of the wagging angle φ and the C═O bond distance R by[55]

$$x = R\varphi \qquad (19)$$

The reciprocal reduced mass expansion g_{44} for this coordinate has the form given in eq 13. The experimentally determined potential energy function for the carbonyl wagging of 3CP is shown in Figure 41. In addition to the potential curve for eq 1, the figure also shows the best fit with a potential energy of the form

$$V = Ax^2 + B \exp(-Cx^2) \qquad (20)$$

where the A, B, and C are potential energy constants. Both eq 1 and eq 20 give very similar results for the energy barrier (939 cm^{-1}), minima ($\pm24°$), and calculated frequencies. The ring-puckering frequency of 127 cm^{-1} in the S$_1$ state is considerably higher than the value of 83 cm^{-1} in the ground state, and this is apparently the result of the asymmetry in the ring-puckering potential function caused by the bending of the C═O group out of plane.

Cyclopentanone (CP). This molecule is different from 3CP in that it is twisted in both its ground and excited states and hence has C$_2$ and C$_1$ symmetry, respectively, for the two states. This means that the FES not only shows transitions to the odd C═O wagging states, but also to the even ones. Figure 42 shows the low-frequency region of the FES of CP[56] which has a band origin of 30,276 cm^{-1}. Several ring-bending bands (ν_{26}) can be

Feature Article

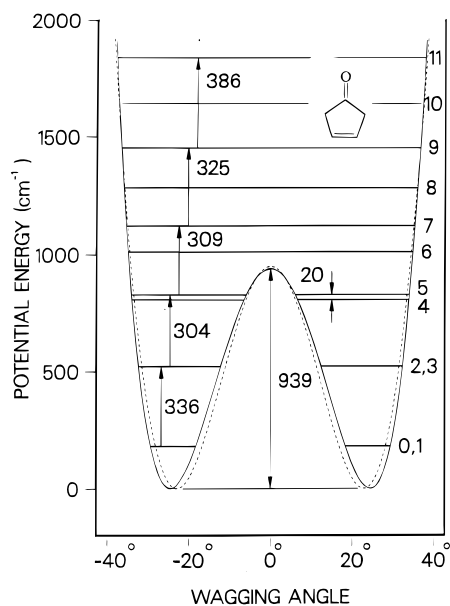*J. Phys. Chem. A, Vol. 104, No. 33, 2000* **7729**

Figure 41. Vibrational potential energy function for the C=O out-of-plane wagging vibration of 3-cyclopenten-1-one. The dashed curve has the form of eq 20.
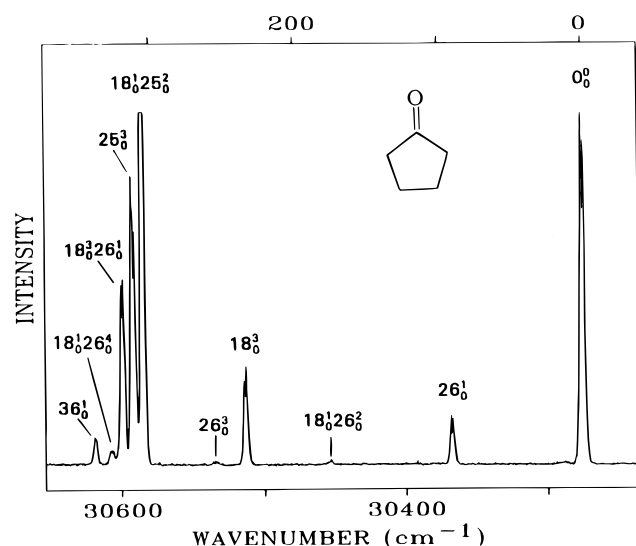

Figure 42. Fluorescence excitation spectra of cyclopentanone.

Figure 43. Energy diagram for low-frequency vibrations of cyclopentanone in its ground and excited states.

Figure 44. Vibrational potential energy function for the C=O out-of-plane wagging vibration of cyclopentanone.

seen as can the splitting of the carbonyl wagging (ν_{25}). Ring-twisting (ν_{18}) bands are also evident. The full spectrum of CP shows nearly a hundred bands below 2000 cm^{-1}, and these were used to create the energy diagram in Figure 43. In the ground state the CP energy levels are doubly degenerate as a result of the barrier to planarity for the ring-twisting mode. In the S$_1$ state the levels become near-4-fold degenerate from the added inversion splitting of the carbonyl wagging. All this data allows us to not only determine the carbonyl wagging potential energy function (Figure 44) with its 680 cm^{-1} barrier, but also makes it possible to determine the two-dimensional potential energy surface for the two out-of-plane ring modes for both electronic states.[56,57] The surface for the excited state is shown in Figure 45. This has a barrier to planarity of 1400 cm^{-1}, which is very similar to the ground-state value, but it has a much lower barrier to interconversion (550 cm^{-1}) from one twisted form to another. In the excited state the ring can invert by passing over a relatively low energy saddle point which corresponds to a bent conformation. This kind of surface helps explain why certain
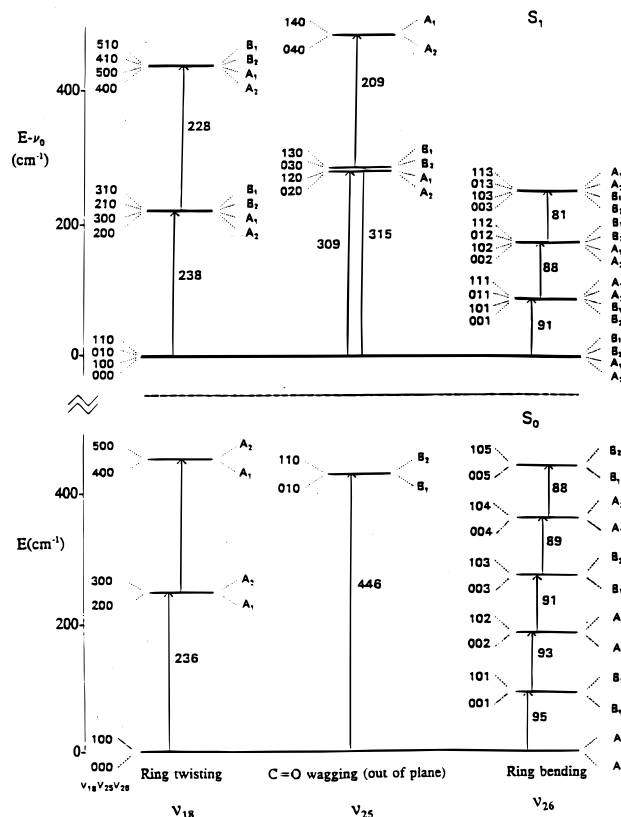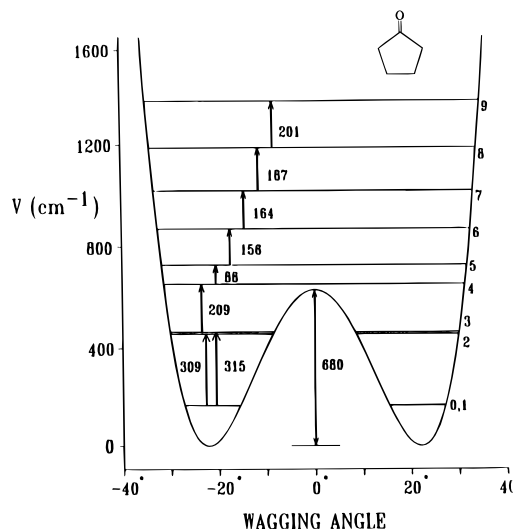
photochemical processes can occur in electronic excited states but cannot in electronic ground states.

Cyclobutanone (CB). The FES of CB[58] is shown in Figure 46, with the band origin at 30,292 cm^{-1}. Only transitions involving the odd quantum levels of the wag are allowed as Type B bands (A$_2$ × B$_2$ = B$_1$ which gives the type B band type). The barrier to inversion of the C=O group of CB is sufficiently high that the lowest six pairs of levels are nearly doubly degenerate with vibrational symmetry species A$_1$ and B$_2$. Even though transitions involving only the vibrational states of B$_2$ symmetry can be observed, these have essentially identical frequencies with those involving the A$_1$ states. Because the C=O group is bent out of the plane in the S$_1$ state, the ring-
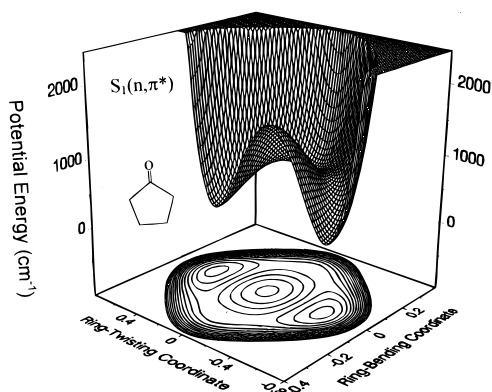
Figure 45. Vibrational potential energy surface for the out-of-plane ring modes of cyclopentanone in its $S_1(n,\pi^*)$ excited electronic state.
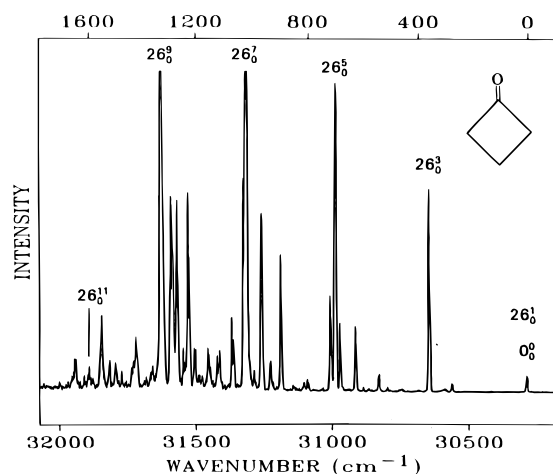

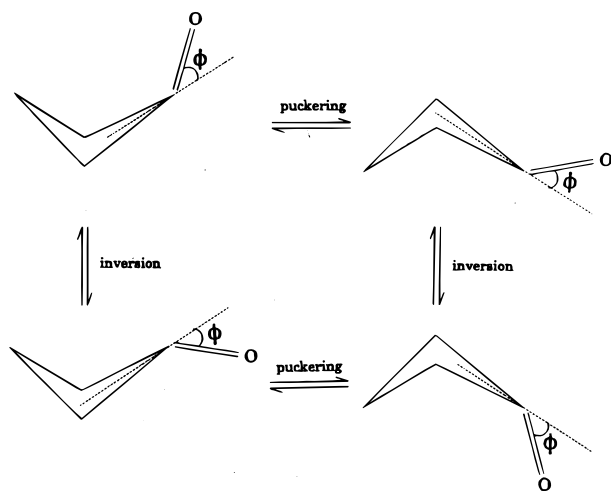**Figure 46.** Fluorescence excitation spectra of cyclobutanone.

Figure 47. Ring-puckering and carbonyl inversion vibrations of cyclobuatanone in its $S_1(n,\pi^*)$ excited electronic state.

puckering motion encounters an asymmetric potential energy surface. This is shown in Figure 47 where puckering toward or away from the bending of the carbonyl group requires a different amount of energy. In the excited state the ring-puckering frequency increases to 106 cm^{-1} from 37 cm^{-1} in the S_0 state and there is sufficient information on the higher levels that a two-dimensional surface in terms of the C=O wagging and puckering can be determined. This surface, which has a barrier to planarity of 2106 cm^{-1} opposing the C=O inversion (a one-dimensional calculation gives a barrier of 2149 cm^{-1}), is shown in Figure 48. The ring is essentially planar (although the energy
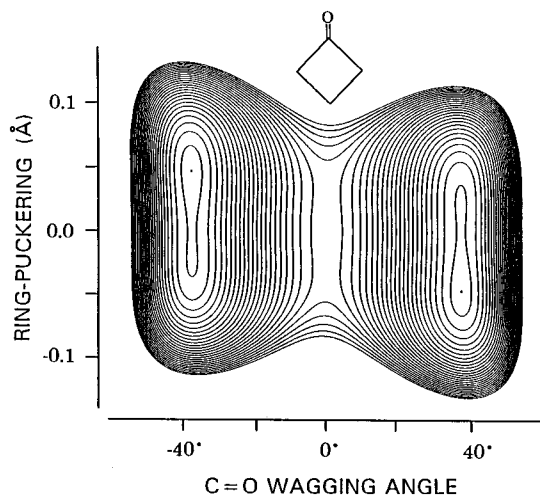

Figure 48. Vibrational potential energy surface for the C=O out-of-plane wagging and ring-puckering vibrations of cyclobutanone.
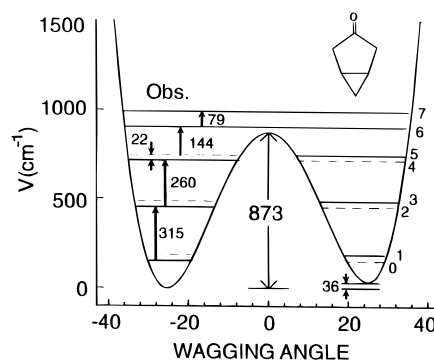

Figure 49. Carbonyl-wagging potential energy function for BCHO in its $S_1(n,\pi^*)$ excited state.

minima correspond to slightly puckered configurations) while the carbonyl group has a wagging angle of $\pm39°$. The effect of the asymmetry is evident in the figure.

Bicyclo[3.1.0]hexan-3-one (BCHO). This molecule is different from the other ketones in that it has a bicyclic ring and that both the ring puckering and carbonyl wagging are asymmetric motions in both the ground and $S_1(n,\pi^*)$ excited electronic states since the three-membered ring is tilted relative to the five-membered ring. The far-infrared spectra were analyzed to determine the ring-puckering potential function in the ground state,[59] and the FES was recorded to determine the puckering and C=O wagging levels in the excited state.[60] The carbonyl wagging potential energy function for the excited state determined from the spectra is shown in Figure 49. The barrier to planarity and energy minima are determined quite well, but the energy difference between the two wells (36 cm^{-1} in the figure) has substantial uncertainty. It is only clear that this value is small (less than 50 cm^{-1}) and the presence of the tilted three-membered ring across from the carbonyl group affects the wagging very little. However, as shown in Figure 50, which compares the ring-puckering potential energy function for the two electronic states, the asymmetry of the molecule has considerably more effect on the puckering motion. Both the ground and excited state functions show substantial asymmetry while that for the excited state shows the ring to become considerably more rigid upon electronic excitation.

Tetrahydrofuran-3-one (THFO) and Tetrahydrothiophen-3-one (THTP). These molecules are similar to cyclopentanone but have either an oxygen or sulfur atom substituted asymmetrically into the five-membered ring. Because of the lack of

Feature Article

J. Phys. Chem. A, Vol. 104, No. 33, 2000 **7731**

TABLE 4: Comparison of Frequencies (cm^{-1}) of Several Vibrations of Cyclic Ketones in Their Ground and S$_1$(n,π*) Electronic Excited States

	2CP		THTP		CP		BCHO		3CP		THFO		CB	
vibration	S$_0$	S$_1$	S$_0$	S$_1$	S$_0$	S$_1$	S$_0$	S$_1$	S$_0$	S$_1$	S$_0$	S$_1$	S$_0$	S$_1$
ring puckering	94	67	67	58	95	91	86	134	83	127	59	82	36	106
ring twisting	287	274	170		38	238			378	377	228	224		
C=O wag o.p.^{a}	537	422	427	326	446	309		315	450	336	463	344	395	355
C=O wag i.p.^{b}	464	348	483	329	467	342			458	339	463	365	454	392
C=O stretch	1748	135	1760	1240	1770	1230			1773	1227	1755	1232	1816	1251
S$_1$ barrier		0		659		672		873		939		1151		2149
v_0^0	27210		30028		30276		30262		30238		30180		30292	

^{a} o.p. = out of plane. ^{b} i.p. = in plane.
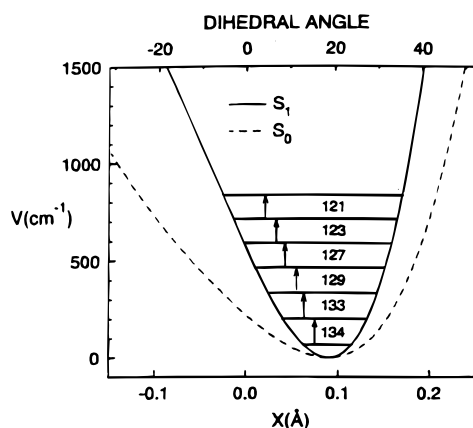
Figure 50. Comparison of the ring-puckering potential energy functions of BCHO in its ground and excited states.
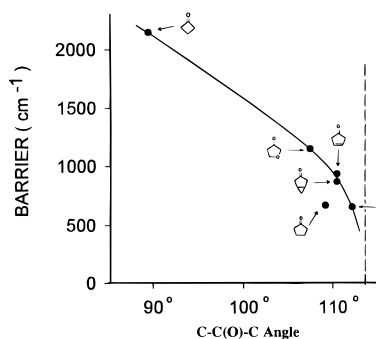
Figure 51. Correlation of inversion barrier with the CCC angle at the carbonyl carbon atom. The dashed line indicates the "strain-free" angle.

symmetry, transitions to each of the carbonyl wagging quantum states are allowed, and the molecules show rich fluorescence excitation spectra[61] from which the carbonyl wagging quantum states in the S$_1$(n,π*) state were determined. These were then used to find the potential energy functions for each molecule using either eq 1 or eq 20. Either type of potential function gives an excellent fit with the experimental data. THFO was found to have a barrier to inversion of 1152 cm^{-1} and energy minima at wagging angles of $\pm26°$ while the corresponding values for THTP are 659 cm^{-1} and $\pm20°$.

Comparison of Molecules. Table 4 summarizes the vibrational frequencies for several of the vibrations of each of these ketones in their ground and excited states. Also shown are the inversion barriers for the excited state and the electronic band origins. Figure 51 correlates the inversion barriers to the interior CCC angle at the carbonyl group of each molecule, as calculated from the MM3 molecular mechanics program. As can be seen, when the interior angle gets smaller and has increased angle strain, the inversion barrier, and hence the degree of bending of the C=O group, increases. Thus, cyclobutanone has the

highest barrier to inversion. This effect follows intuition in that closing the CCC angle allows more bending of the carbonyl group. This is similar to what has been observed for the HCH angles in cyclopropane, cyclobutane, and cyclopentane; namely, the HCH angle is largest for cyclopropane and smallest for cyclopentane.[62]

V. Summary

In this article we have examined the electronic excited states of three different types of molecules. In each case we have spectroscopically established the vibronic quantum states for conformationally important low-frequency vibrations and used these with our computer programs to determine the vibrational potential energy surfaces which govern the conformational processes. Although interactions between electronic excited states and other complicating factors might be expected to make these types of studies much less feasible, we have been pleasantly surprised that much of the methodology we have developed for analyzing electronic ground states is also applicable to the excited states.

For the indan family of molecules, previous investigations, which attempted to utilize one-dimensional potential energy functions to explain the spectra, resulted in flawed interpretations. For these molecules it is essential to utilize two-dimensional analyses considering the strongly interacting ring-flapping and ring-puckering motions. In order to understand the electronic excited state data, it is also essential to have the ground state problem solved correctly. The fluorescence excitation spectra of the jet-cooled molecules clearly help to identify which transitions originate from the vibrational ground states in the S$_0$ states. Because of Franck–Condon factors these generally show transitions to only a few of the vibronic levels in the S$_1$(π,π*) states. The ultraviolet absorption spectra recorded at ambient temperatures, however, show transitions originating from many upper ring-puckering or flapping levels in S$_0$, and, hence, show transitions to many of the higher vibronic levels which must be considered for meaningful interpretations of the excited electronic state potential energy surfaces. Thus, all four types of spectra shown in Figure 4 must be utilized to complete studies of this type. The far-infrared and Raman data make it possible to analyze the electronic ground state, without which the interpretation of the electronic absorption spectra is nearly impossible. This is demonstrated by the fact that the previously recorded electronic spectra of the molecules discussed in this article were generally incorrectly analyzed. Just the identification of the electronic band origin has often been a problem.

The results obtained for phthalan were somewhat unexpected. It is not clear why this molecule should have a tiny barrier to planarity in the electronic ground state and why this should disappear as the five-membered ring becomes more rigid in its S$_1$(π,π*) state. However, ab initio calculations also predict this

tiny barrier. In fact, for all the molecules in the indan family, ab initio calculations do a remarkable job in predicting the barriers for the ground electronic states. The results for 1,3-benzodioxole are perhaps the most interesting. The barrier in the electronic ground state is clearly due to a suppressed anomeric effect, as is supported by the ab initio calculations. The magnitude of this effect is reduced by interactions between the benzene ring and the oxygen atom orbitals in the five-membered ring. In the $S_1(\pi,\pi^*)$ state, however, the transition to the antibonding orbital results in reduced π character in the benzene ring and reduces the interaction with the oxygen atoms. This reduces the suppression of the anomeric effect and the barrier to planarity increases. We are currently investigating other molecules with the anomeric effect and with oxygen atoms next to benzene rings to see if suppression of the anomeric effect for ground-state molecules is decreased by electronic excitation.

For *trans*-stilbene the presence of eight low-frequency vibrations complicated the analysis of the spectra considerably. However, the high-temperature Raman spectra of the vapor went a long way toward clarifying the assignments. The dispersed fluorescence spectra then allowed the excited vibrational quantum states for the torsional vibrations to be established and these were utilized to determine the potential energy surfaces for the electronic ground state. Once the S_0 levels were known, the assignment of the $S_1(\pi,\pi^*)$ levels was considerably simplified. The analyses required five separate computer programs to be written for the calculation of the kinetic energy and potential energy surfaces for the phenyl torsions and the C=C torsion. What is remarkable is how well all the data could be fit with relatively few parameters and assumptions.

The fluorescence excitation spectra of the cyclic ketones involving the transitions to the $S_1(n,\pi^*)$ states are considerably weaker than those where π to π^* transitions are involved. Moreover, the dispersed fluorescence spectra are also very weak. However, the transitions involving the out-of-plane carbonyl wagging motion are typically the strongest in the spectra, and, hence, quite easy to identify. Thus, we have been able to determine the carbonyl wagging potential functions and barriers to inversion for six ketones discussed here. For most of these, as well as for 2-cyclopenten-1-one, which has a conjugated carbonyl group and lacks a double-minimum potential function, we have also been able to analyze the out-of-plane ring modes and ring conformations in the electronic excited state.

Our experimental results, which provide accurate comparisons for the various conformational energies of a molecule are invaluable for checking the quality of ab initio calculations. For the electronic ground state we have found that the agreement between the experiments and the computations is remarkably good. However, for electronic excited states the computational methodology required to get good results remains to be sorted out. Nonetheless, our experimental results provide the conformational energy data which future ab initio calculations should be able to reproduce.

The molecules we have studied so far have electronic absorption bands in the 27,000–38,000 cm^{-1} range. The addition of our new OPO laser system will extend our operational range to beyond 45 000 cm^{-1} and will permit us to study additional electronic states and additional kinds of molecules, many of which have interesting photochemical properties resulting from structural and bonding changes in electronic excited states. The use of two-photon spectroscopy will also allow us to probe deeper into the ultraviolet region. Molecules with two or more chromophores, which may be interacting with one another, will also be the focus of future investigations.

References and Notes

(1) Laane, J. *Pure Appl. Chem.* **1987**, *59*, 1307.

(2) Laane, J. In *Structures and Conformations of Non-Rigid Molecules*; Laane, J., Dakkouri, M., van der Veken, B., Oberhammer, H., Eds.; Elsevier: Amersterdam, 1993; Chapter 4.

(3) Laane, J. *Annu. Rev. Phys. Chem.* **1994**, *45*, 179.

(4) Laane, J. *Int. Rev. Phys. Chem.* **1999**, *18*, 301.

(5) Bell, R. P. *Proc. R. Soc.* **1945**, *A183*, 328.

(6) Laane, J.,*J. Phys. Chem.* **1991**, *95*, 9246.

(7) Laane, J. *Appl. Spectrosc.* **1970**, *24*, 73.

(8) Klots, T.; Lee, S. N.; Laane, J. *J. Phys. Chem.* **1999**, *103*, 833.

(9) Laane, J. *J. Chem. Phys.* **1969**, *50*, 776.

(10) Borgers, R. R.; Strauss, H. L. *J. Chem. Phys.* **1966**, *45*, 947.

(11) Irwin, R. M.; Cooke, J. M.; Laane, J. *J. Am. Chem. Soc.* **1977**, *99*, 3273.

(12) Laane, J.; Lord, R. C. *J. Chem. Phys.* **1967**, *47*, 4941.

(13) Laane, J.; Lord, R. C. *J. Chem. Phys.* **1968**, *48*, 1508.

(14) Malloy, T. B. *J. Mol. Spectrosc.* **1972**, *44*, 504.

(15) Laane, J.; Harthcock, M. A.; Killough, P. M.; Bauman, L. E.; Cooke, J. M. *J. Mol. Spectrosc.* **1982**, *91*, 286.

(16) Harthcock, M. A.; Laane, J. *J. Mol. Spectrosc.* **1982**, *91*, 300.

(17) Schmude, R. W.; Harthcock, M. A.; Kelly, M. B.; Laane, J. *J. Mol. Spectrosc.* **1987**, *124*, 369.

(18) Tecklenburg, M. M.; Laane, J. *J. Mol. Spectrosc.* **1989**, *137*, 65.

(19) Strube, M. M.; Laane, J. *J. Mol. Spectrosc.* **1988**, *129*, 126.

(20) Cheatham, C. M.; Huang, M.-H.; Laane, J. *J. Mol. Struct.* **1996**, *377*, 93.

(21) Cheatham, C. M.; Huang, M.-H.; Meinander, N.; Kelly, M. B.; Haller, K.; Chiang, W.-Y.; Laane, J. *J. Mol. Struct.* **1996**, *377*, 81.

(22) Morris, K. Ph.D. Thesis, Texas A&M University, 1999. Morris, K.; Laane, J., to be published.

(23) Klots, T.; Sakurai, S.; Laane, J. *J. Chem. Phys.* **1998**, *108*, 3531.

(24) Sakurai, S.; Meinander, N.; Laane, J. *J. Chem. Phys.* **1998**, *108*, 3537.

(25) Bondoc, E.; Sakurai, S.; Morris, K.; Chiang, W.-Y.; Laane, J. *J. Chem. Phys.*, in press.

(26) Sakurai, S.; Meinander, N.; Morris, K.; Laane, J. *J. Am. Chem. Soc.* **1999**, *121*, 50.

(27) Laane, J.; Bondoc, E.; Sakurai, S.; Morris, K.; Meinander, N.; Choo, J. *J. Am. Chem. Soc.* **2000**, *122*, 2628.

(28) Bondoc, E.; Klots, T.; Laane J. *J. Phys. Chem.* **2000**, *104*, 275.

(29) Takayanagi, M.; Hanazaki, I. *Chem. Phys. Lett.* **1993**, *208*, 5.

(30) Smithson, T. L.; Duckett, J. A.; Wieser, H. *J. Phys. Chem.* **1984**, *88*, 102.

(31) Hassan, K. H.; Hollas, J. M. *J. Mol. Spectrosc.* **1991**, *147*, 100.

(32) Caminati, W.; Damiani, D.; Corbelli, G.; Favero, L. B. *Mol. Phys.* **1992**, *75*, 857.

(33) Moon, S.; Kwon, Y.; Lee, J.; Choo, J. *J. Phys. Chem.*, in press.

(34) Cortez, E.; Verastegui, R.; Villarreal, J. R.; Laane, J. *J. Am. Chem. Soc.* **1993**, *115*, 12132.

(35) Green, W. H. *J. Chem. Phys.* **1969**, *50*, 1619

(36) Chiang, W.-Y.; Laane, J. *J. Chem. Phys.* **1994**, *101*, 8755, and references therein.

(37) Waldeck, D. H. *Chem. Rev.* **1991**, *91*, 415, and references therein.

(38) Banares, L.; Heikal, A. A.; Zewail, A. H. *J. Chem. Phys.* **1992**, *96*, 4127.

(39) Haller, K.; Chiang, W.-Y.; del Rosario, A.; Laane J. *J. Chem. Phys.* **1996**, *379*, 19.

(40) Chiang, W.-Y.; Laane, J. *J. Phys. Chem.* **1995**, *99*, 11823.

(41) Walsh, A. D. *J. Chem. Soc.* **1953**, 2306.

(42) Brand, J. C. D. *J. Chem. Soc.* **1956**, 858.

(43) Rao, V. R.; Rao, I. A. *Indian J. Phys.* **1954**, *28*, 491.

(44) Innes, K. K.; Giddings, L. E. *J. Mol. Spectrosc.* **1961**, *7*, 435.

(45) Hubbard, L. M.; Bocian D. F.; Birge, R. R. *J. Am. Chem. Soc.* **1981**, *103*, 3313.

(46) Noble, M.; Lee, E. K. C. *J. Chem. Phys.* **1984**, *81*, 1632.

(47) Baba, M.; Hanazaki, I.; Nagashima, U. *J. Chem. Phys.* **1985**, *82*, 3938.

(48) Noble, M.; Apel, E. C.; Lee, E. K. C. *J. Chem. Phys.* **1983**, *78*, 2219.

(49) Gordon, R. D.; Orr, D. R. *J. Mol. Spectrosc.* **1988**, *129*, 24.

(50) Howard-Lock, H. E.; King, G. W. *J. Mol. Spectrosc.* **1970**, *36*, 53.

(51) Moule, D. C. *J. Chem. Phys.* **1976**, *64*, 3161.

(52) Cheatham, C. M.; Laane, J. *J. Chem. Phys.* **1991**, *94*, 7743.

(53) Cheatham, C. M.; Laane, J. *J. Chem. Phys.* **1991**, *94*, 5394.

(54) Sagear, P.; Laane, J. *J. Chem. Phys.* **1995**, *102*, 7789.

(55) Laane, J.; Harthcock, M. A.; Killough, P. M.; Bauman, L. E.; Cooke, J. M. *J. Mol. Spectrosc.* **1982**, *91*, 286.

(56) Zhang, J.; Chiang, W.-Y.; Laane, J. *J. Chem. Phys.* **1993**, *98*, 6129.

(57) Choo, J.; Laane, J. *J. Chem. Phys.* **1994**, *101*, 2772.

(58) Zhang, J.; Chiang, W.-Y.; Laane, J. *J. Chem. Phys.* **1994**, *100*, 3455.

(59) Choo, J.; Chiang, W.-Y.; Lee, S. N.; Laane, J. *J. Phys. Chem.* **1995**, *99*, 11636.

(60) Chiang, W.-Y.; Laane, J. *J. Phys. Chem.* **1995**, *99*, 11640.

(61) Sagear, P. A.; Lee, S. N.; Laane, J. *J. Chem. Phys.* **1997**, *106*, 3876.

(62) Yamamoto, S.; Nakata, M.; Fukuyama, T.; Kuchitsu, K. *J. Phys. Chem.* **1985**, *89*, 3298.